Title

Use of recombinant microRNAs as antimetabolites to inhibit human non-small cell lung cancer



Journal

Acta Pharmaceutica Sinica B, 13(10)

ISSN

2211-3835

Authors

Chen, Yixin

Tu, Mei-Juan

Han, Fangwei

et al.

Publication Date

2023-10-01

DOI

10.1016/j.apsb.2023.07.011

Peer reviewed

Acta Pharmaceutica Sinica B 2023;13(10):4273–4290

Chinese Pharmaceutical Association
Institute of Materia Medica, Chinese Academy of Medical Sciences

Acta Pharmaceutica Sinica B

www.elsevier.com/locate/apsb
www.sciencedirect.com

ORIGINAL ARTICLE

# Use of recombinant microRNAs as antimetabolites to inhibit human non-small cell lung cancer

**Yixin Chen[a,b], Mei-Juan Tu[a], Fangwei Han[c], Zhenzhen Liu[a], Neelu Batra[a], Primo N. Lara[d], Hong-Wu Chen[a], Huichang Bi[b], Ai-Ming Yu[a,*]**

[a]*Department of Biochemistry and Molecular Medicine, School of Medicine, UC Davis, Sacramento, CA 95817, USA*
[b]*School of Pharmaceutical Sciences, Sun Yat-sen University, Guangzhou 510006, China*
[c]*School of Public Health, UNT Health Science Center, Fort Worth, TX 76107, USA*
[d]*Department of Internal Medicine, School of Medicine, UC Davis, Sacramento, CA 95817, USA*

Received 4 December 2022; received in revised form 13 March 2023; accepted 18 May 2023

**KEY WORDS**

RNA therapy;
Folate metabolism;
Amino acid;
Glycolysis;
miR-22;
miR-9;
miR-218;
Lung cancer

**Abstract** During the development of therapeutic microRNAs (miRNAs or miRs), it is essential to define their pharmacological actions. Rather, miRNA research and therapy mainly use miRNA mimics synthesized *in vitro*. After experimental screening of unique recombinant miRNAs produced *in vivo*, three lead antiproliferative miRNAs against human NSCLC cells, miR-22-3p, miR-9-5p, and miR-218-5p, were revealed to target folate metabolism by bioinformatic analyses. Recombinant miR-22-3p, miR-9-5p, and miR-218-5p were shown to regulate key folate metabolic enzymes to inhibit folate metabolism and subsequently alter amino acid metabolome in NSCLC A549 and H1975 cells. Isotope tracing studies further confirmed the disruption of one-carbon transfer from serine to folate metabolites by all three miRNAs, inhibition of glucose uptake by miR-22-3p, and reduction of serine biosynthesis from glucose by miR-9-5p and -218-5p in NSCLC cells. With greater activities to interrupt NSCLC cell respiration, glycolysis, and colony formation than miR-9-5p and -218-5p, recombinant miR-22-3p was effective to reduce tumor growth in two NSCLC patient-derived xenograft mouse models without causing any toxicity. These results establish a common antifolate mechanism and differential actions on glucose uptake and metabolism for three lead anticancer miRNAs as well as antitumor efficacy for miR-22-3p nanomedicine, which shall provide insight into developing antimetabolite RNA therapies.

*Corresponding author.
E-mail address: aimyu@ucdavis.edu (Ai-Ming Yu).

Peer review under the responsibility of Chinese Pharmaceutical Association and Institute of Materia Medica, Chinese Academy of Medical Sciences.

https://doi.org/10.1016/j.apsb.2023.07.011

## 1. Introduction

Lung cancer is the most common type of cancer, and it remains the leading cause of cancer deaths among men and women in the United States and worldwide that is more than breast, prostate, and colon cancer deaths combined[1,2]. Over 85% of lung cancer cases are defined as non-small cell lung cancer (NSCLC), and the majority of patients usually suffer from advanced diseases or complications[3]. Current pharmacotherapies for unresectable or advanced lung cancer include chemotherapies, targeted therapies, and the most recent immunotherapies which all have their utilities and certain limitations, such as a low response rate and an inevitable presence or development of resistance[4], leading to an overall five-year survival rate of 19% for all lung cancer diagnoses[1]. Therefore, it is essential to explore common pharmacological mechanisms towards the development of more effective therapies and/or precision medications for the treatment of NSCLC.

Dysregulated carcinoma cells are usually subjected to greater degrees of transport and metabolism of key nutrients to fuel the synthesis of critical biomolecules required for rapid proliferation[5]. Notably, glycolysis is preferably utilized in carcinoma cells over oxidative phosphorylation in normal cells for mitochondrial production of energy-carrying molecules (*i.e.*, ATP) in the presence of oxygen, which the former is known as "Warburg effect" or aerobic glycolysis in highly proliferative cancer cells[6]. Meanwhile, many intermediate metabolites derived from glycolysis provide abundant and essential building blocks (*e.g.*, amino acids) for cancer cells to synthesize macromolecules (*e.g.*, proteins). Therefore, many transporters and enzymes involved in glycolysis, such as the glucose transporter protein type 1 (GLUT1 or SLC2A1), are commonly upregulated in carcinoma cells including NSCLC, representing potential targets for the development of new anticancer therapies[7]. Folate metabolism is another notable pathway usually upregulated in cancer cells, and it is characterized by the activation and transfer of one-carbon methylene unit from serine into folate metabolites to support nucleic acid biosynthesis, redox defense, and epigenetic maintenance, and contribute to amino acid homeostasis[8,9]. Indeed, some anticancer medications have been revealed to interfere with folate and/or nucleic acid metabolism to exert their pharmacological effects, such as the folic acid derivatives aminopterin and methotrexate that inhibit dihydrofolate reductase (DHFR) to generate tetrahydrofolate (THF)[10], 5-fluorouracil that inhibits thymidylate synthase (TYMS or TS) to produce dihydrofolate and deoxythymidine monophosphate[11], and pemetrexed that blocks DHFR, TS, and glycinamide ribonucleotide formyltransferase[12], for the treatment of various types of malignancies including lung cancer[13].

Aberrant expression of some functional microRNAs (miRNAs or miRs) has been demonstrated in NSCLC cells and patient samples[14−16], which belong to a superfamily of small non-protein-coding RNAs (ncRNAs) around 18−25 nucleotides in length that are derived from the human genome to control posttranscriptional gene regulation through translation inhibition or mRNA degradation mechanisms[17]. Certain miRNAs (*e.g.*, miR-7-5p) have been identified to act on various targets (*e.g.*, EGFR and YAP[18,19]) to modulate important cancer cellular processes, such as metabolism, proliferation, apoptosis, invasion, metastasis, tumorigenicity, and resistance[16,20,21]. Control of cancer cell metabolism by specific miRNAs[20,22] generally involve posttranscriptional regulation of respective nutrient transporters (*e.g.*, GLUT1 by miR-22-3p[23]) and/or metabolic enzymes (*e.g.*, methylenetetrahydrofolate dehydrogenase (MTHFD) by miR-22-3p[24]). It is noteworthy that some miRNAs, such as miR-7-5p[25], miR-22-3p[26−28], miR-124-3p[29,30], let-7-5p[31,32], and miR-218-5p[33−35], have been consistently shown to be downregulated or lost in NSCLC tumor tissues while acting as tumor suppressors, while there are some discrepancies on a few other miRNAs, such as miR-9-5p[36−38]. Therefore, efforts are underway to develop means to effectively reintroduce such tumor suppressive miRNAs into tumor cells to achieve anticancer therapy[39−41]. This "miRNA replacement therapy" strategy is more attractive than "antagonism" of oncogenic miRNAs overexpressed in NSCLC because miRNAs are safe components in normal cells, and reintroduction of miRNAs may be more tolerable in subjects than exogenous antagomirs[39−41].

To understand miRNA functions and develop miRNA therapies, we have established a one-of-a-kind, *in vivo* fermentation-based approach to attain high-yield and large-scale production of recombinant or bioengineered miRNA molecules, namely BERAs[42], which are distinguished from conventional miRNA agents (*e.g.*, miRNA mimics) synthesized chemically or enzymatically *in vitro*. Produced and folded in living cells *in vivo* and only comprised of natural posttranscriptional modifications[43,44], BERAs are true biologic RNA molecules and expected to better recapitulate the structures, functions, and safety profiles of natural RNAs for research and development[45]. To increase the biocompatibility to human cells, specific human tRNAs (htRNA) (*e.g.*, leucyl tRNA or htRNA$^{Leu}$) have been further identified to replace bacterial tRNA within the tRNA/hsa-pre-miRNA carrier to offer fully humanized, bioengineered miRNA agents (hBERAs)[46]. In addition to being precisely processed to target miRNAs to selectively regulate the expression of targeted genes in human cells, recombinant BERA/miRNA and hBERA/miRNA agents are effective to control tumor progression and metastasis in xenograft tumor mouse models[47−50].

In this study, folate one-carbon metabolism was disclosed for the first time through bioinformatic studies as one major targeted cluster for top six most effective miRNAs against NSCLC cell viability identified by experimental screening of a small, focused group of unparalleled recombinant miRNAs. Among them, multiple folate metabolic enzyme-encoding genes were computationally predicted and experimentally validated as direct targets for three lead miRNAs, miR-22-3p, -9-5p, and -218-5p. Consequently, the three miRNAs were shown to remarkably suppress folate metabolism, including the incorporation of isotope labeled one-carbon unit from serine to folate metabolites, and alter the amino acid metabolome in both A549 and H1975 cells. In addition, the three miRNAs were found to differentially regulate the expression of glucose transporter and serine biosynthesis enzymes to modulate glucose uptake, conversion into serine, and overall glycolytic capacity. Among them, miR-22-3p was revealed as the most effective

to inhibit one-carbon metabolism, leading to the greatest reduction of NSCLC cell energetics and colony formation as well as induction of cell cycle arrest, and thus the effectiveness and safety of recombinant miR-22-3p therapy to control tumor growth was unprecedentedly established in two NSCLC patient-derived xenograft (PDX) mouse models *in vivo*. These findings demonstrate the importance of folate one-carbon metabolism in NSCLC, improving the understanding of miRNA mechanistic actions in the control of NSCLC cell metabolism and supporting the development of miR-22-3p therapy for the treatment of NSCLC.

## 2. Materials and methods

### 2.1. Production of fully humanized bioengineered RNA agents (hBERA)

The expression and purification of hBERA/miRNAs and the control RNA (Sephadex aptamer tagged $htRNA^{leu}$) were carried out as we described recently[46]. Briefly, each RNA expressing plasmid was constructed by inserting the coding sequence (Supporting Information Table S1) of target miRNA accommodated in an optimal $htRNA^{leu}$/pre-miR-34a carrier (Fig. 1A) into pBSMrna vector using specific primers (Supporting Information Table S2) and In-Fusion cloning technology (Takara, USA). Individual plasmids were confirmed by DNA sequencing analyses (Genscript, USA). Recombinant RNAs were expressed in *Escherichia coli* HST08 (Clontech, USA), and total bacterial RNAs were insolated through phenol extraction. Recombinant RNAs were purified with an anion exchange fast protein liquid chromatography (FPLC) method[43,46] (Supporting Information Fig. S1) on an NGC QUEST 10PLUS system (Bio-Rad, USA). The purity of each hBERA was validated by denaturing urea (8 mol/L) polyacrylamide (8%) gel electrophoresis (PAGE) and quantitatively determined by the high-performance liquid chromatography (HPLC) analysis[43] on a Prominence Ultra-Fast LC system (Shimadzu Corporation, Japan). Endotoxin levels were determined by using a Limulus Amebocyte Lysate Pyrpgent-5000 kinetic assay kit (Lonza, USA). hBERAs showing >98% purity and <5 EU/μg RNA (Supporting Information Fig. S2A and S2B) were used for the following studies, which were selectively processed to target miRNAs (Fig. S2C) in human NSCLC cells.

### 2.2. Cell culture and transfection

The human NSCLC cell lines A549 (ATCC Cat# CCL-185) and H1975(ATCC Cat# CRL-5908) as well as embryonic kidney 293 cell line (ATCC Cat# CRL-3216) were purchased from American Type Culture Collection. The cells were maintained in RPMI-1640 or DMEM medium (Gibco, USA) with glucose, L-glutamine and sodium pyruvate supplemented with 10% fetal bovine serum (Gibco, USA) at 37 °C in a humidified atmosphere of 5% $CO_2$ and 95% air. Cells within the logarithmic growth phases were transfected with hBERAs (for 72 h unless specified) or plasmids (for 48 h) by using Lipofectamine 3000 reagent (Invitrogen, USA) with the reduced serum medium Opti-MEM (Gibco, USA) and following the manufacturer's protocols.

### 2.3. RNA isolation and quantitative real-time PCR analysis

Cells were seeded into 12-well plates and then transfected with 15 nmol/L of miRNAs, control RNA or lipofectamine 3000 reagent only (Vehicle control) for 72 h. Total RNA was extracted with the Direct-zol RNA MiniPrep Kit (Zymo Research, USA) and quantified with a microplate reader (TECAN, USA). Single-stranded complementary DNA was synthesized by reverse transcription (RT) reaction using NxGen M-MuLV reverse transcriptase (Lucigen, USA) and stem-loop primers or random hexamers primers. The real-time qPCR analyses were conducted on a CFX96 Touch Real-time PCR system (Bio-Rad, USA) with iTaq™ Universal SYBR Green Supermix (Bio-Rad, USA) according to the manufacturer's protocols. The fold changes were analyzed using the ΔΔCt method as reported[46]. Sequences of primers used for RT and qPCR reactions are provided in Supporting Information Tables S3 and S4.

### 2.4. Gene enrichment analysis and pathway analysis

To identify common target genes and related pathways for the most effective anti-tumor miRNAs, the gene enrichment analysis and pathway analysis were performed. First, candidate miRNAs were input into the MIENTURNET database (MicroRNA Enrichment TURned NETwork, http://userver.bio.uniroma1.it/apps/mienturnet/), and 4000 potential target genes were enriched. Second, all enriched genes meeting the criteria (*i.e.*, have top 1000 smallest OR and FDR; have at least two miRNA-target interactions) were selected manually to prepare the gene-set for the KEGG pathway analysis. Finally, a gene concept network was applied to determine the involved genes and the relationships among top 20 pathways after KEGG pathway enrichment analysis.

### 2.5. Protein isolation and Western blot analysis

Cells were seeded into 6-well plates and then treated with 15 nmol/L of miRNAs, control RNA or vehicle for 72 h. Cells were lysed by using RIPA buffer containing complete protease inhibitors, and protein concentrations were determined with a BCA Protein Assay Kit (Thermo Fisher Scientific, USA). Thirty micrograms of proteins per lane were separated on a 10% SDS-PAGE gel and electrophoretically transferred onto polyvinylidene fluoride membranes. After blocking with 5% nonfat milk, membranes were incubated with primary antibodies against SHMT-1 (1:1000, Abcam Cat# ab186130), MTHFR (1:1000, Abcam Cat# ab203786), MTHFD2 (1:1000, Cell Signaling Technology Cat# 41377), MTHFD1L (1:1000, Cell Signaling Technology Cat# 14999), GLUT1 (1:2000, Abcam Cat# ab32551), ACTB (1:1000, Santa Cruz Biotechnology Cat# sc-8432) or GAPDH (1:1000, Santa Cruz Biotechnology Cat# sc-47724) overnight at 4 °C, followed by an incubation with the secondary anti-mouse or anti-rabbit antibodies (1:5000, Cell Signaling Technology, Cat# 7076 or Cat# 7074) at room temperature. The ECL detection substrates (Bio-Rad, USA) were applied to develop the blots, and the images were obtained with a ChemiDoc MP Imaging System (Bio-Rad). The intensity values of the protein bands were determined by the Image J software and normalized to corresponding GADPH or ACTB levels for comparison.

### 2.6. MRE site identification and dual luciferase reporter gene assay

The gene coding sequences of mRNA 3′UTR segment consisting of MREs (miRNA response elements) were identified by TargetScan database. Specifically, MREs for miR-9-5p are within

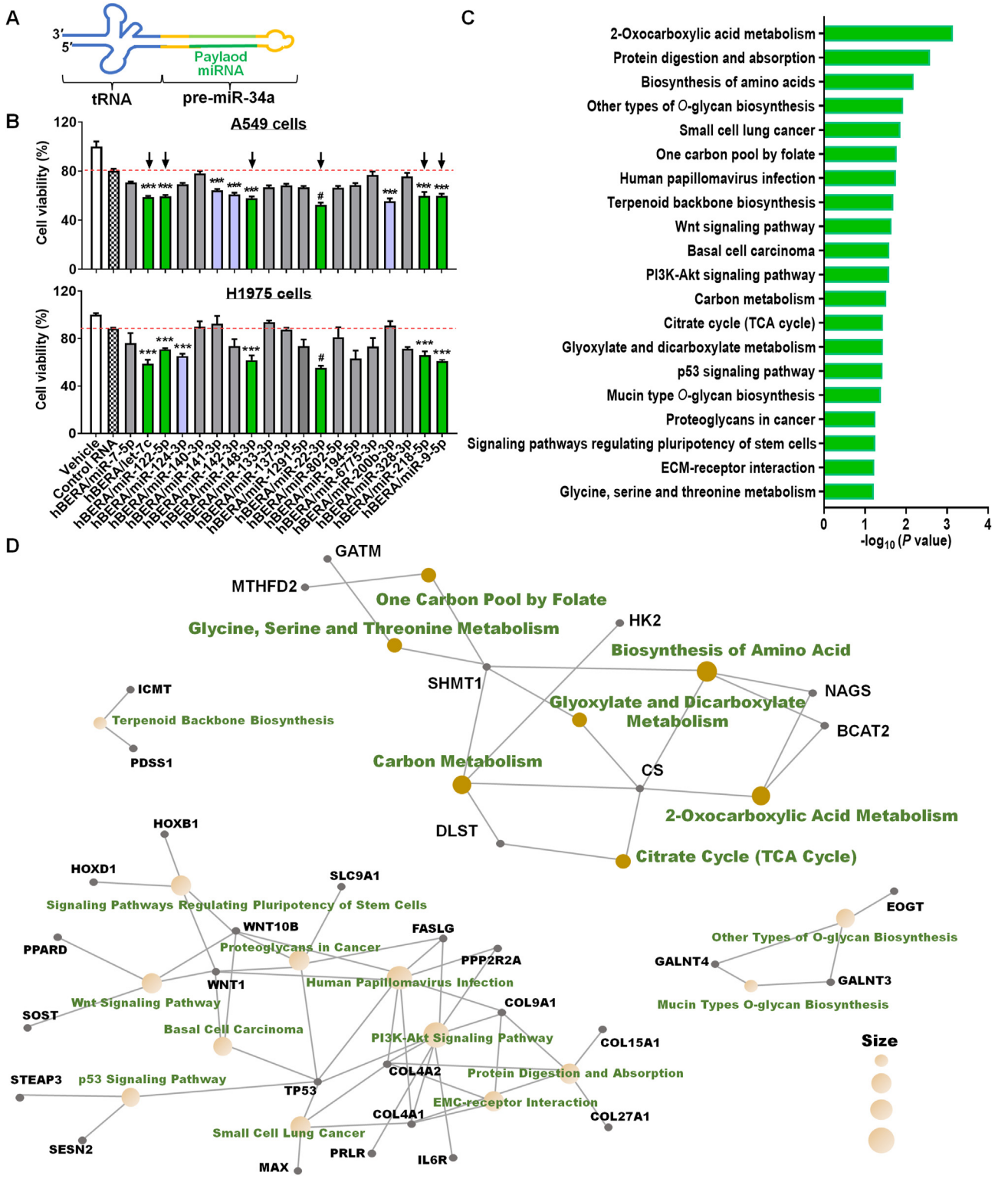


**Figure 1** Experimental screening and computational analyses reveal antifolate a common action for lead antiproliferative miRNAs against NSCLC cells. (A) Schematic illustration of novel recombinant miRNA agents based on an optimal carrier, hsa-pre-miR-34a fused to human leucyl tRNA (htRNA$^{Leu}$), in which the miR-34a duplexes are replaced by payload miRNAs. (B) The top six most effective hBERA/miRNAs (highlighted in Green) in the inhibition of both A549 and H1975 cell viability were identified from a focused set of hBERAs (15 nmol/L). Control RNA and vehicle treatments were included for comparison, and values are mean ± SD ($n$ = 5/group). ***$P < 0.001$ and $^{\#}P < 0.0001$, compared with control RNA (one-way ANOVA with Bonferroni *post hoc* tests). (C) Top 20 enriched pathways for the six miRNAs revealed by miRNA-target gene enrichment analysis and KEGG pathway analysis. (D) A Gene-Concept Network plot highlights the relationships of those enriched pathways and their associated genes, among which the one-carbon folate metabolism stands out as a major cluster.

the 3′UTR of *SHMT-1, MTHFD2* and *MTHFD1L*. MREs for miR-218-5p are within the *SHMT-1* 3′UTR and MREs for miR-22-3p are within the *MTHFR* and *MTHFD2* 3′UTR. Individual reporter plasmids were constructed by cloning full-length 3′UTR segments into the downstream of the firefly luciferase gene within the Pezx-MT06 vector (Genecopoeia, USA). Luciferase reporter assays were performed as described previously[51], in which the firefly and *Renilla* (internal control) luciferase activities were determined by a commercial Dual-Luciferase Reporter Assay Kit (Promega, USA) on the Spark multimode microplate reader (Tecan, USA), according to the manufacturer's protocols.

### 2.7. LC−MS/MS quantification of folate metabolites, amino acids, and glucose

All analytes were quantified by using multiple-reaction monitoring (MRM) method in positive electrospray ionization (ESI) mode and optimal conditions on a Shimadzu Prominence Ultra-Fast Liquid Chromatography system coupled to an AB Sciex 4000 QTRAP mass spectrometry (AB SEIEX, USA).

Standard folate metabolites, including folic acid, DHF, THF, 5,10-methylene-THF, 5-methyl-THF, 5,10-methenyl-THF and 5-formyl-THF, were purchased from the Schricks Laboratory (Bauma, Switzerland). A 50 mmol/L HEPES buffer (pH 8.0) containing 1% ascorbic acid and 1% $\beta$-mercaptoethanol (Sigma−Aldrich, USA) was used for sample preparation as well as folate metabolite standard solutions to maintain their stabilities and optimal conditions[52]. Cells were seeded into 10-cm plates and treated with 15 nmol/L of miRNAs, control RNA or vehicle for 72 h. Cell pellets resuspended in 150 μL HEPES buffer were subjected to three cycles of probe-sonication and vortex, followed by normalization with protein concentration, and addition of internal standard (IS) working solution (10 μL of 0.1 μmol/L 4-chloro-phenylalanine in HEPES buffer). Sixty μL of activated charcoal-treated rat plasma was added to each sample, and the mixture was incubated at 37 °C for 4 h. After centrifugation, 200 μL of acetonitrile was added into the supernatant to precipitate the sample. Addition of another 400 μL HEPES buffer made the acetonitrile concentration in the sample 25%. After vortex and centrifugation, the mixture was loaded onto an Isolute PLD$^+$ protein removal column (Biotage, Sweden), and the filtrate was collected, centrifuged, and transferred to new tube for LC−MS/MS analysis of folate metabolites with a F5 column (50 mm × 2.1 mm, 2.6 μm; Kinetex, USA) and gradient elution at 0.4 mL/min flow rate. Specifically, the mobile phases were comprised of 0.5% formic acid in water (solution A) and 0.5% formic acid in acetonitrile (solution B). Column was eluted with 60% solution B for 1.5 min, which was increased to 95% solution B from 1.5 min to 3.5 min, maintained at 95% for 1.5 min, then returned to initial 100% solution A condition in 1 min and maintained for another 2 min. Data were acquired and processed with the Analyst software (AB SCIEX). The chemical formula as well as optimal MRM and mass spectrometry conditions for individual folate metabolites are provided in Supporting Information Table S5, and LC−MS/MS traces and calibration curves of individual folate metabolites are shown in Supporting Information Fig. S5.

Quantification of individual amino acids was conducted by using the LC−MS/MS method we reported very recently[51,53] after cells were treated with 15 nmol/L of miRNAs, control RNA or vehicle in 6-well plates for 72 h. Likewise, an Intrada Amino Acid column (50 mm × 3 mm, 3 μm; Imtakt, USA) was utilized for LC−MS/MS analysis of glucose and uniformly labelled glucose ($^{13}$C) levels as well as corresponding $^{13}$C-labeled serine metabolite in separate batches of cells by using the optimized method we reported recently[51,54], except that MRM transitions are unique for $^{13}$C-labeled glucose (185.1 → 92.1) and serine (109.0 → 62.1).

### 2.8. Glucose uptake assay

Cells were seeded in 96-well plates and transfected with 15 nmol/L of miR-22-3p, control RNA or vehicle for 72 h. Cells were washed twice with 37 °C glucose free KRB (KrebseRinger Bicarbonate) buffer at pH 7.4[54], and preincubated with the buffer for 15 min in a 5% $CO_2$ incubator at 37 °C. Then the incubation buffer was discarded and replaced with 100 mL KRB buffer supplemented with 600 mmol/L 2-NBDG (2-[*N*-(7-nitrobenz-2-oxa-1,3-diazol-4-yl) amino]-2-deoxyglucose) (Thermo Fisher Scientific, USA) and incubated at 37 °C for 30 min. After three washes with ice-cold PBS, another 100 mL PBS was added. The fluorescence intensity was measured immediately on a SpectraMax Microplate Reader at 465/540 nm excitation/emission wavelength. Cells were further lysed with SDS, and protein concentration of each sample was determined by BCA assay to normalize the glucose uptake capacity.

### 2.9. Real-time live cell mitochondrial function and glycolysis

The oxygen consumption rates (OCR) and extracellular acidification rates (ECAR) were measured using a Seahorse XFe24 analyzer (Agilent, USA). Briefly, after 48 h treatment with 15 nmol/L of miRNAs, control RNA or vehicle, 5000 cells/well were seeded into XFe-24 well cell culture plates and incubated overnight. On the following day, the medium was replaced with Seahorse assay medium supplemented with 10 mmol/L glucose, 1 mmol/L Pyruvate, and 2 mmol/L L-glutamine, and then incubated at 37 °C without $CO_2$ for 30 min. By using the Agilent Seahorse XF Glycolytic Rate Assay Kit (103344-100) and following the User Guide, proton efflux rates (PER) were determined. Likewise, the mitochondrial respiratory capacity was assessed as described in the User Guide of Agilent Seahorse XF Cell Mito Stress Test Kit (103015-100). All data were normalized to corresponding protein concentrations that were determined with BCA Protein Assay Kit.

### 2.10. ROS and NADP/NADPH ratio assays

Cells were seeded into 96-well plates and treated with 15 nmol/L of miRNAs, control RNA or vehicle for 72 h. ROS levels were determined with a Fluorometric Intracellular ROS Kit (Sigma−Aldrich, USA). Cells were pretreated with DCFH-DA working solution in a 5% $CO_2$ 37 °C incubator for 1 h and then detected with a fluorescence microplate reader (Tecan, USA) at an excitation wavelength of 540 nm and an emission wavelength of 570 nm. The intracellular NADP/NADPH ratio was determined with a NADP/NADPH-Glo assay kit (Promega, USA), according to the manufacturer's protocol after transfection with 15 nmol/L of miRNAs, control RNA or vehicle. Similarly, cells were incubated with the NADP/NADPH-Glo™ Detection Reagent and shaken gently. After 45 min incubation at room temperature, the luminescence signals were recorded by a microplate reader (Tecan, USA).

### 2.11. Cell viability assay and colony formation analysis

To screen the panel of recombinant miRNAs in the inhibition of NSCLC cell viability, cells were seeded into 96-well plates and treated with 15 nmol/L individual miRNAs, control RNA or vehicle. Cell viability was measured by the addition of 10 μL MTT (5 mg/mL) reagent to each well at 72 h post-transfection and incubation for 4 h. The absorbance was measured at wavelengths of 570 and 630 nm following adding and incubating with 200 μL DMSO. For miR-22-3p, miR-9-5p, and miR-218-5p, further cell viability studies were performed by using a CellTiter-Glo Luminescent cell viability assay kit (Promega, USA) after treating cells with various concentrations of miRNAs (0, 5, 10, 15, 20 nmol/L) for 72 h.

Colony formation analysis was conducted by seeding 2000 cells in each 6-well plate well after transfection with 15 nmol/L of individual miRNAs, control RNA or vehicle for 72 h and allowing the cells to form colonies for 2 weeks. The cells were fixed with ethanol, stained with 0.1% crystal violet reagent for 5 min, and counted using a stereomicroscope.

### 2.12. Flow cytometry analyses

Cells were seeded into 6-well plates and transfected with 15 nmol/L of miRNAs, control RNA or vehicle for 72 h. To examine the effects of miRNAs on cell cycle, cells were fixed with 70% cold ethanol and then stained with the PI/RNase Staining Buffer (BD Biosciences, USA). Samples were analyzed on a FAC-Scan flow cytometer (BD Biosciences, USA) at a 488 nm wavelength. All data were processed with FlowJo Version 10.6.2.

### 2.13. Immunofluorescence study

Cells were plated in an 8-well chamber slide and treated with 15 nmol/L of miRNAs, control RNA or vehicle for 72 h. To determine the expression levels of cell cycle marker Cyclin A2, cells were fixed with 4% paraformaldehyde. After being permeabilized and blocked, cells were incubated with a primary antibody (Thermo Fisher Scientific Cat# MA1-154) overnight at 4 °C, followed by the incubation with anti-mouse Alexa Fluor 488-conjugated secondary antibody (Thermo Fisher Scientific Cat# A55058). DAPI (Catalog #4083, Cell Signaling Technology) was added to cells to stain the nuclei. All images were obtained by using Zeiss Axio Observer.zl Microscope coupled to a Zeiss LSM 710 Scanning Device (Zeiss, Germany).

### 2.14. Therapy study in NSCLC patient-derived xenograft (PDX) mouse model

All animal procedures were approved by the Institute Animal Care and Use Committee at University of California, Davis (UC Davis). Lung adenocarcinoma PDX tissues, namely LG-1202 and LG-0552F that were generated with de-identified tumor specimens from a 47-year-old White female and a 63-year-old American Indian male, respectively, were obtained from the Mouse Biology Shared Resources at UC Davis Cancer Center as a joint program with The Jackson Laboratory (USA). PDX tissues were thawed and minced into 2−3 $mm^3$ pieces and then subcutaneously implanted into the right flank of six-week-old male SCID mice (The Jackson Laboratory, USA). The body weights and the tumor sizes were monitored twice a week, and the tumor volumes were calculated based on Eq. (1):

$$\text{Tumor volumes } (mm^3) = 0.52 \times [\text{Length (mm)} \times \text{Width}^2\ (mm^2)] \quad (1)$$

When the tumor volumes reached 80−120 $mm^3$, tumor-bearing mice were randomized into two groups (6 mice/group) to receive either hBERA/miR-22-3p or control RNA (30 μg a time, twice a week, intravenous injection *via* tail vein) that were formulated with liposome-polyethylenimine nanocomplexes as we described previously[48,49,55]. The animals were treated for a total of four (for LG-0552F PDX mice) or five (LG-1202) weeks and then euthanized after one week from the last dose. Mouse whole blood and tumor samples were collected for serum biochemistry analyses and histopathological studies, respectively (UC Davis Comparative Pathology Laboratory). Tumor samples were also processed for Western blot assays to examine the pharmacological actions of biologic miR-22-3p agent.

### 2.15. Statistical analysis

All values are mean ± standard deviation (SD). Two-tailed Student's *t*-tests, 1-way or 2-way ANOVA with Bonferroni *post hoc* tests were used to assess the differences (Prism 8.0, GraphPad Software, USA). Statistical significance is noted as $^{*}P < 0.05$, $^{**}P < 0.01$, $^{***}P < 0.001$, and $^{\#}P < 0.0001$. Each experiment was repeated at least three times independently.

## 3. Results

### 3.1. Identification of common actions for the top antiproliferative miRNAs through screening of novel bioengineered miRNA agents and bioinformatic analyses

A set of novel recombinant miRNA molecules, namely hBERA/miRNAs, were first overexpressed heterogeneously in bacteria and purified to a high degree of homogeneity by using our unique RNA bioengineering technology[46] to screen for potent inhibitors against human NSCLC cell viability, including miR-22-3p, miR-9-5p, miR-218-5p, and miR-1291-5p that were first reported in current study (Table S1). In particular, the optimal $htRNA^{leu}$/hsa-pre-miR-34a carrier was employed to accommodate target miRNA duplexes (Fig. 1A). After the RNA-expressing plasmids were designed and cloned using specific primers (Table S2) and verified by DNA sequencing, individual plasmids were transformed into *E. coli* to achieve overexpression of target hBERA/miRNAs which were readily validated by urea-PAGE analysis of total bacterial RNAs (Supporting Information Fig. S1A). Recombinant miRNA molecules were then purified with an anion exchange FPLC method[46,51] (Fig. S1B). The quality of final biologic miRNA agents was determined by HPLC analysis and endotoxin assay, showing a high purity (>98%) and low endotoxin levels (<5 EU/μg RNA), respectively (Supporting Information Fig. S2A and S2B). In addition, selective stem-loop RT-qPCR analyses (Supporting Information Table S3) were carried out to verify the selective release of target miRNAs from hBERAs in human NSCLC A549 and H1975 cells, as manifested by a sharp increase of miR-22-3p, miR-9-5p, and miR-218-5p in cells treated with corresponding hBERA/miRNAs (Fig. S2C).

Cell viability assay was then performed to compare the effectiveness of a small set of tumor suppressive miRNAs against NSCLC (Fig. 1B). Among them, six recombinant miRNAs at 15 nmol/L concentration, let-7c-5p, miR-9-5p, miR-22-3p,

miR-122-5p, miR-148-3p, and miR-218-5p, were identified to inhibit both A549 and H1975 cell viability by more than 30%. Therefore, the miRNA-target gene enrichment analysis and KEGG pathway analysis were performed to explore possible common targets for the six miRNAs (Supporting Information Fig. S3). The top 20 enriched pathways were shown in a bar plot (Fig. 1C), and a Gene-Concept Network plot was further constructed to demonstrate the relationships of those enriched pathways and their associated genes, in which the node size reflects the number of connected genes (Fig. 1D). The clustering of certain pathways closely related to tumor metabolism stood out, especially the folate one-carbon metabolism that was subjected to extensive investigation in this study.

### 3.2. *Several key folate metabolic enzymes are direct targets of miR-22-3p, -9-5p, and -218-5p*

Because folate one-carbon metabolism was revealed as one major cluster behind six most effective antiproliferative miRNAs (Fig. 1), specific folate metabolic enzyme-encoding genes were identified explicitly as direct targets for three of the six miRNAs, miR-22-3p, miR-9-5p, and miR-218-5p (Fig. 2A). In particular, the SHMT1 3′UTR contains one MRE for miR-218-5p and another MRE for miR-9-5p, and MTHFD2 is comprised of two MREs for miR-22-3p and two MREs for miR-9-5p. Meanwhile, miR-22-3p may act on the 3′UTR of MTHFR, and miR-9-5p may interact with MTHFD1L. A series of dual luciferase reporter assays were thus conducted, and the suppression of target 3′UTR luciferase activities by individual miRNAs validated their interactions, including miR-218-5p with SHMT1, miR-22-3p with MTHFD2 and MTHFR, and miR-9-5p with SHMT1, MTHFD1L, and MTHFD2 (Fig. 2B). Furthermore, the impact of each miRNA on the protein outcome of corresponding target gene was determined by immunoblot analysis (Fig. 2C). In both A549 and H1975 cells, biologic miR-218-5p was effective to reduce SHMT1 protein levels by about 60%−90%, as compared with control RNA or vehicle treatments. Likewise, miR-22-3p significantly inhibited both MTHFD2 and MTHFR protein levels, and miR-9-5p repressed SHMT1, MTHFD1L, and MTHFD2 protein levels in A549 and H1975 cells. Together, these results demonstrate that multiple key enzymes within the folate cycle are directly regulated by three lead miRNAs, miR-22-3p, miR-9-5p, and miR-218-5p.

### 3.3. *MiR-22-3p, -9-5p, and -218-5p disrupt folate one-carbon metabolism in NSCLC cells*

Given the roles for miR-22-3p, -9-5p and -218-5p in the regulation of folate metabolic enzyme expression, we were motivated to delineate to what degrees individual miRNAs would alter folate metabolism. A selective and accurate LC−MS/MS method was thus developed to simultaneously quantitate multiple major folate metabolites within the folate cycle, including folic acid, DHF, THF, 5-methyl-THF, 5,10-methenyl-THF, and 5-formyl-THF (Fig. 3A). As reported[52,56], the HEPES buffer was used for sample preparation in which 5,10-methylene-THF was indeed degraded quickly (Supporting Information Fig. S4A), and thus it was not included in the method. Final extracts were stored in HEPES buffer consisting of 25% acetonitrile to maintain folate metabolite stability and injected for LC−MS/MS analyses. Using specific MRM transitions and optimal MS/MS conditions (Supporting Information Table S4), individual folate metabolites were detected selectively following the liquid chromatography separation (Fig. S4B), and calibration curves were established to cover broad ranges of concentrations with excellent regression coefficients ($R^2 > 0.99$) (Fig. S4C).

This LC−MS/MS method was then employed to determine the impact of miRNAs on folate metabolite profiles in NSCLC cells. The data showed that miR-22-3p, -9-5p, and -218-5p all significantly increased folic acid and DHF contents in both A549 and H1975 cells (Fig. 3B), indicating the suppression of folic acid and DHF entering the folate cycle by individual miRNAs. Consistently, the levels of folate metabolites, 5-methyl-THF and 5,10-methenyl-THF, were obviously reduced by all the three miRNAs in both cell lines. Interestingly, while miR-22-3p and miR-9-5p dramatically decreased THF concentrations and slightly reduced 5-formyl-THF levels, miR-218-5p elevated THF levels and had no effects on 5-formyl-THF contents (Fig. 3B), which is likely attributable to the fact that miR-218-5p only targets SHMT1 in the folate cycle, whereas miR-22-3p and -9-5p each regulates multiple folate metabolic enzymes (MTHFD2 and MTHFR or MTHFD1L) (Fig. 2). Overall, miR-22-3p inhibited folate metabolism to the greatest degree among the three lead miRNAs, as indicated by the lowest THF, 5-methyl-THF, 5,10-methenyl-THF, and 5-formyl-THF levels in both A549 and H1975 cells following miR-22-3p treatments (Fig. 3B).

To examine the influence of miRNAs on precise incorporation of the one-carbon unit, namely methylene group or bridge, from serine into the folate cycle, a feeding experiment was conducted by using isotope-labelled serine ($^{13}$C, D, $^{15}$N), and corresponding metabolites 5-methyl-THF (M+3) and 5,10-methenyl-THF (M+2) formed from intermediate 5,10-methylene-THF (M+3) by MTHFR and MTHFD, respectively (Fig. 3C), were determined by LC−MS/MS analysis. The data showed that recombinant miR-22-3p, -9-5p, and -218-5p all significantly decreased 5-methyl-THF (M+3) and 5,10-methenyl-THF (M+2) levels in both A549 and H1975 cells, compared with control RNA or vehicle treatments (Fig. 3D), demonstrating the inhibition of integration of serine methylene bridge into the folate cycle by all three miRNAs. Taken together, the results reveal that miR-22-3p, -9-5p, and -218-5p all exhibit antifolate activities, among which miR-22-3p is the most effective.

### 3.4. *Change of amino acid metabolome by miR-22-3p, -9-5p, and -218-5p in NSCLC cells*

Given the interplay between folate cycle and amino acid catabolism as well as the complexity of aminolyses[57,58], we subsequently investigated the influence of three lead miRNAs on the homeostasis of endogenous amino acids in NSCLC cells by using a selective and accurate LC−MS/MS method described very recently[51,53]. While individual amino acid levels were largely variable and most amino acids were not altered dramatically by any of the three miRNAs in A540 and H1975 cells, intracellular serine and glycine concentrations were remarkably lower in miR-9-5p- and -218-5p-treated cells, and extracellular serine and glycine levels were much higher in miR-9-5p- and -218-5p-treated cells than respective control RNA or vehicle treatment groups (Fig. 4A). Interestingly, miR-22-3p altered the methionine homeostasis, as indicated by the reduction of intracellular methionine levels and elevation of extracellular methionine contents. Nevertheless, the decrease of intracellular endogenous serine levels was rather opposing to our hypothesis because the enzyme SHMT1 catalyzing serine one-carbon transfer to folate metabolites was directly regulated by miR-9-5p and miR-218-5p (Fig. 2).

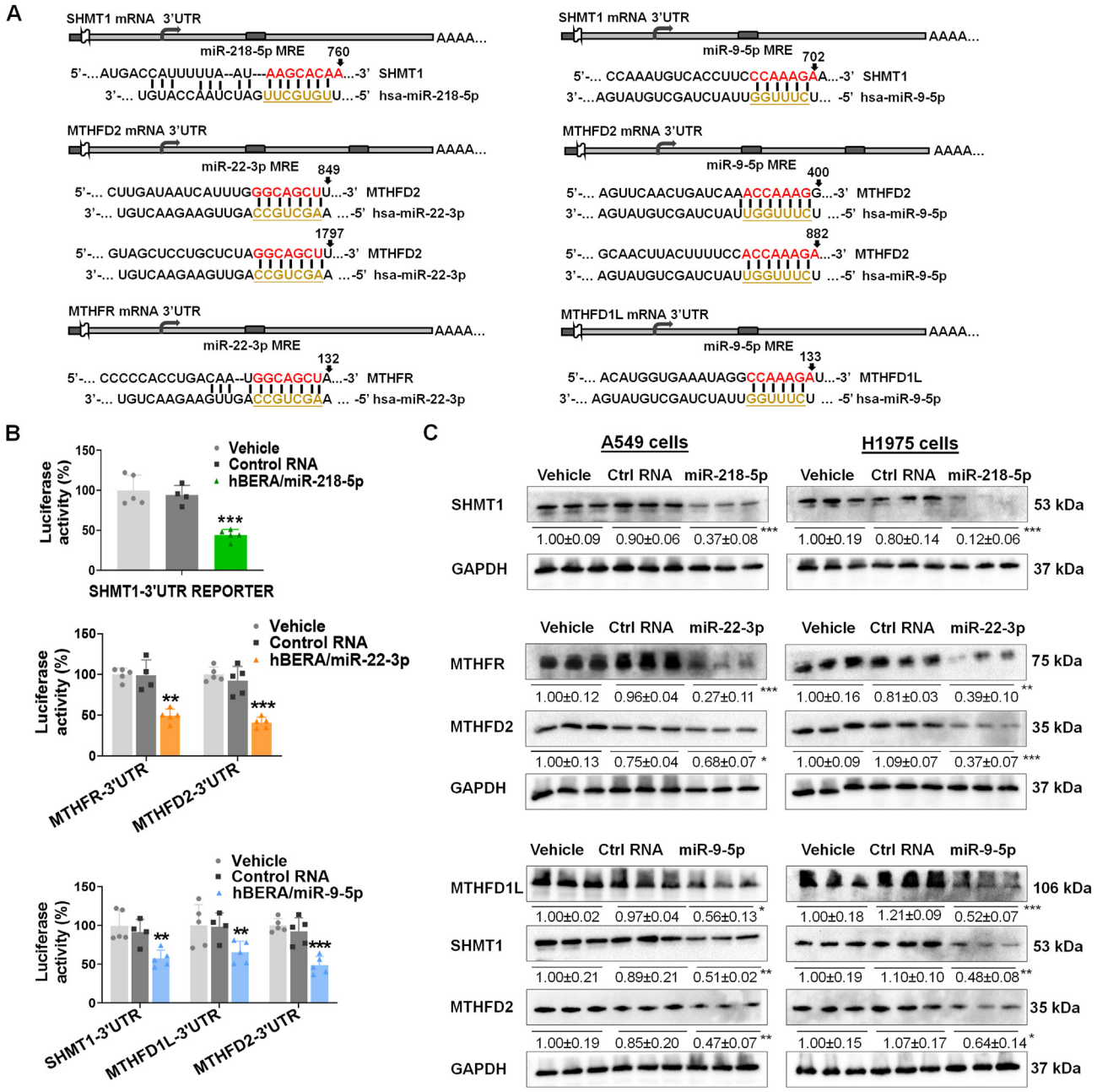


**Figure 2** MiR-22-3p, miR-9-5p, and miR-218-5p control the expression of multiple folate-metabolizing enzymes in human NCSLC cells. (A) SHMT1 was identified as a putative target for miR-218-5p, and SHMT1, MTHFD1L and MTHFD2 for miR-9-5p, as well as MTHFR and MTHFD2 for miR-22-3p. Underlined are the seed sequences of individual miRNAs that interact with corresponding MREs *via* complimentary base pairing. SHMT1: serine hydroxymethyltransferase 1, MTHFD2: methylenetetrahydrofolate dehydrogenase 2, MTHFR: methylenetetrahydrofolate reductase, MTHFD1L: methylenetetrahydrofolate dehydrogenase 1 like. (B) Dual luciferase reporter assay validated the interactions between individual pairs of miRNAs and target genes. Values are mean ± SD ($n$ = 5/group). (C) The protein levels of SHMT1, MTHFD1L, MTHFD2, and MTHFR were determined in A549 and H1975 cells by Western blot analyses. Cells were treated with 15 nmol/L of hBERA/miRNAs, control RNA or vehicle for 72 h. GAPDH was used as a loading control for data normalization. Values are mean ± SD ($n$ = 3/group). $^{*}P < 0.05$, $^{**}P < 0.01$, and $^{***}P < 0.001$, compared with respective control RNA treatment (one- or two-way ANOVA with Bonferroni *post hoc* tests).

Therefore, isotope-labelled serine ($^{13}$C, D, $^{15}$N) was added into cell culture medium to validate the effects of miR-9-5p and -218-5p on serine depletion (Fig. 4B) in NSCLC cells. The data showed that, compared with control RNA or vehicle treatments, miR-9-5p and miR-218-5p treatments indeed increased the levels of both intracellular and extracellular isotope-labelled serine ($^{13}$C, D, $^{15}$N) in A549 and H1975 cells (Fig. 4C). These results indicate a reduction of serine expenditure and one-carbon metabolism by miR-9-5p and miR-218-5p, as well as inhibition of methionine consumption by miR-22-3p, in NSCLC cells.

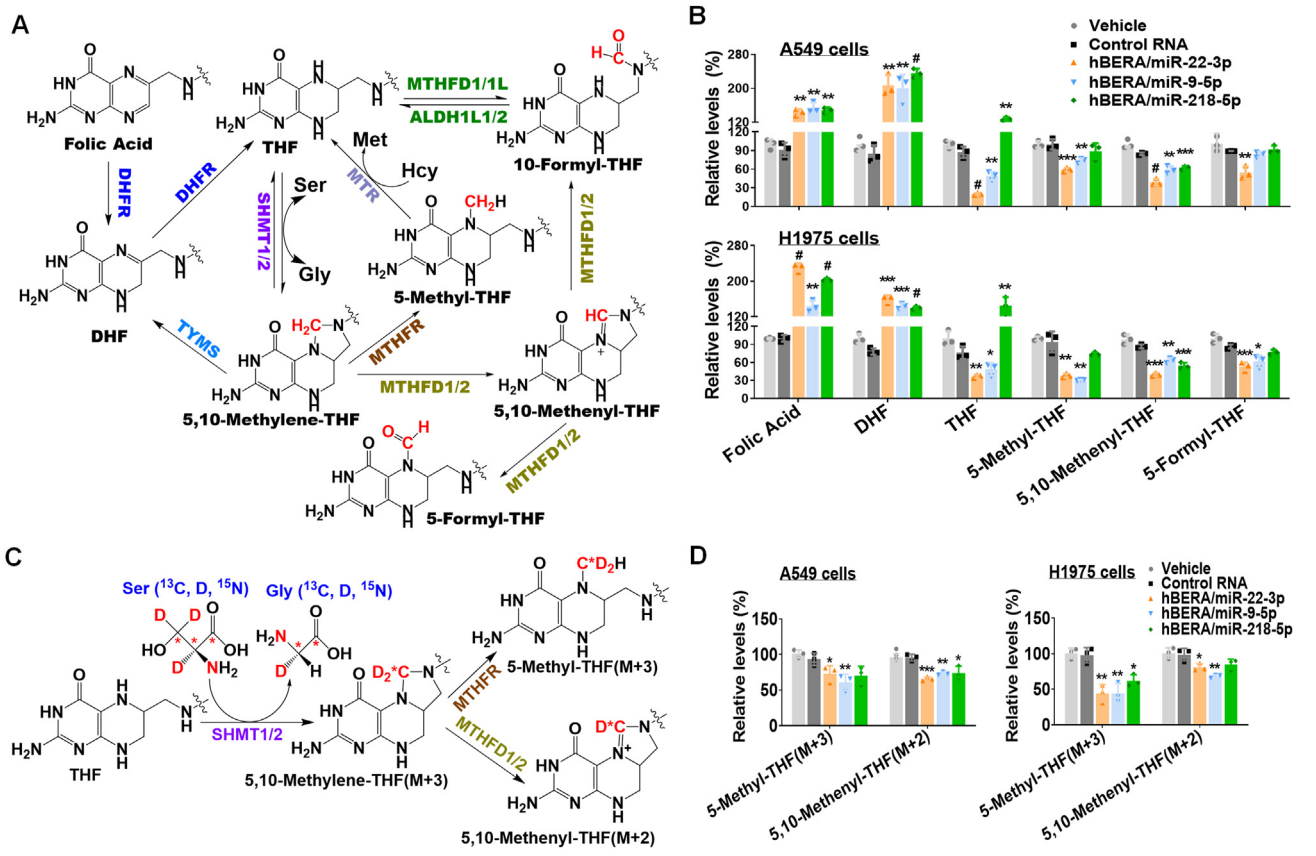


**Figure 3** Antifolate effects of miR-22-3p, miR-9-5p, and miR-218-5p in human NSCLC cells. (A) Schematic representation of the folate cycle and chemical structures of folate metabolites. DHFR, dihydrofolate reductase; ALDH1L1, 10-formyltetrahydrofolate dehydrogenase; MTR, methionine synthase; MTHFD1, methylenetetrahydrofolate dehydrogenase 1; SHMT1, cytosolic form of serine hydroxymethyltransferase; MTHFR, methylene tetrahydrofolate reductase; SHMT2, mitochondrial form of serine hydroxymethyltransferase; MTHFD2, mitochondrial bifunctional methylenetetrahydrofolate dehydrogenase/cyclohydrolase; MTHFD2L, methylenetetrahydrofolate dehydrogenase 2-like protein; ALDH1L2, aldehyde dehydrogenase 1 family, member L2, the mitochondrial isoform of ALDH1L1; MTHFD1L, mitochondrial monofunctional C1-tetrahydrofolate synthase; TYMS, thymidylate synthase; DHF, dihydrofolate; THF, tetrahydrofolate; Ser, serine; Gly, glycine; Met, methionine; Hcy, homocysteine. (B) Intracellular folate metabolite (Folic acid, DHF, THF, 5-methyl-THF, 5,10-methenyl-THF, and 5-formyl-THF) contents were determined in A549 and H1975 cells by selective LC−MS/MS method after cells were treated with 15 nmol/L of hBERA/miRNAs, control RNA or vehicle for 72 h. Values are mean ± SD ($n$ = 3/group). (C) Schematic diagram of the incorporation of one-carbon unit from serine to folate metabolites. (D) Intracellular 5-methyl-THF (M+3) and 5,10-methenyl-THF (M+2) were quantified by LC−MS/MS method after replacing serine with isotope-labeled serine ($^{13}$C, D, $^{15}$N) in cell culture medium. Cells were treated with 15 nmol/L of bioengineered miRNAs, control RNA or vehicle for 72 h. Values are mean ± SD ($n$ = 3/group). $^{*}P < 0.05$, $^{**}P < 0.01$, $^{***}P < 0.001$, and $^{\#}P < 0.0001$, compared with control RNA (two-way ANOVA with Bonferroni *post hoc* tests).

### *3.5. Different actions of miR-22-3p, -9-5p, and -218-5p in the control of glucose uptake and biotransformation to serine, and influence on glycolysis capacity in NSCLC cells*

Given the findings that miR-9-5p and miR-218-5p reduced the depletion of isotope-labelled serine, whereas overall endogenous serine levels were lower within cells, we reasoned that serine biosynthesis from glucose (Fig. 5A) might be affected. In addition, the glucose transporter GLUT1 (Fig. 5A) has been validated as a direct target for miR-22-3p in breast cancer cells[23]. Therefore, we employed the uniformly labelled glucose ($^{13}$C) to feed NSCLC cells to determine the impact of miR-22-3p, -9-5p, and -218-5p on glucose uptake and conversion into respective $^{13}$C-labeled serine. The data (Fig. 5B) showed that, compared with respective control RNA treatments, intracellular $^{13}$C-glucose levels decreased by around 30% and 60% in miR-22-3p-treated A549 and H1975 cells, respectively, which were accompanied by similar extents of decrease in intracellular $^{13}$C-serine levels. By contrast, while intracellular $^{13}$C-glucose concentrations remained unchanged, the intracellular $^{13}$C-serine levels were reduced to approximately 40%−60% by miR-9-5p and -218-5p in A549 and H1975 cells, as compared to control RNA or vehicle treatments (Fig. 5B). The results indicate that miR-9-5p and -218-5p inhibit the serine biosynthesis from glucose while miR-22-3p directly reduces the glucose uptake.

The impact of miR-22-3p on glucose uptake was further confirmed by using the 2-NBDG-based glucose uptake assay, which revealed a significant suppression of glucose uptake by recombinant miR-22-3p in both A549 and H1975 cells (Fig. 5C). Moreover, the downregulation of GLUT1 transporter by miR-22-3p in NSCLC cells was demonstrated by immunoblot analyses (Fig. 5D). On the other hand, to explore the mechanism by which

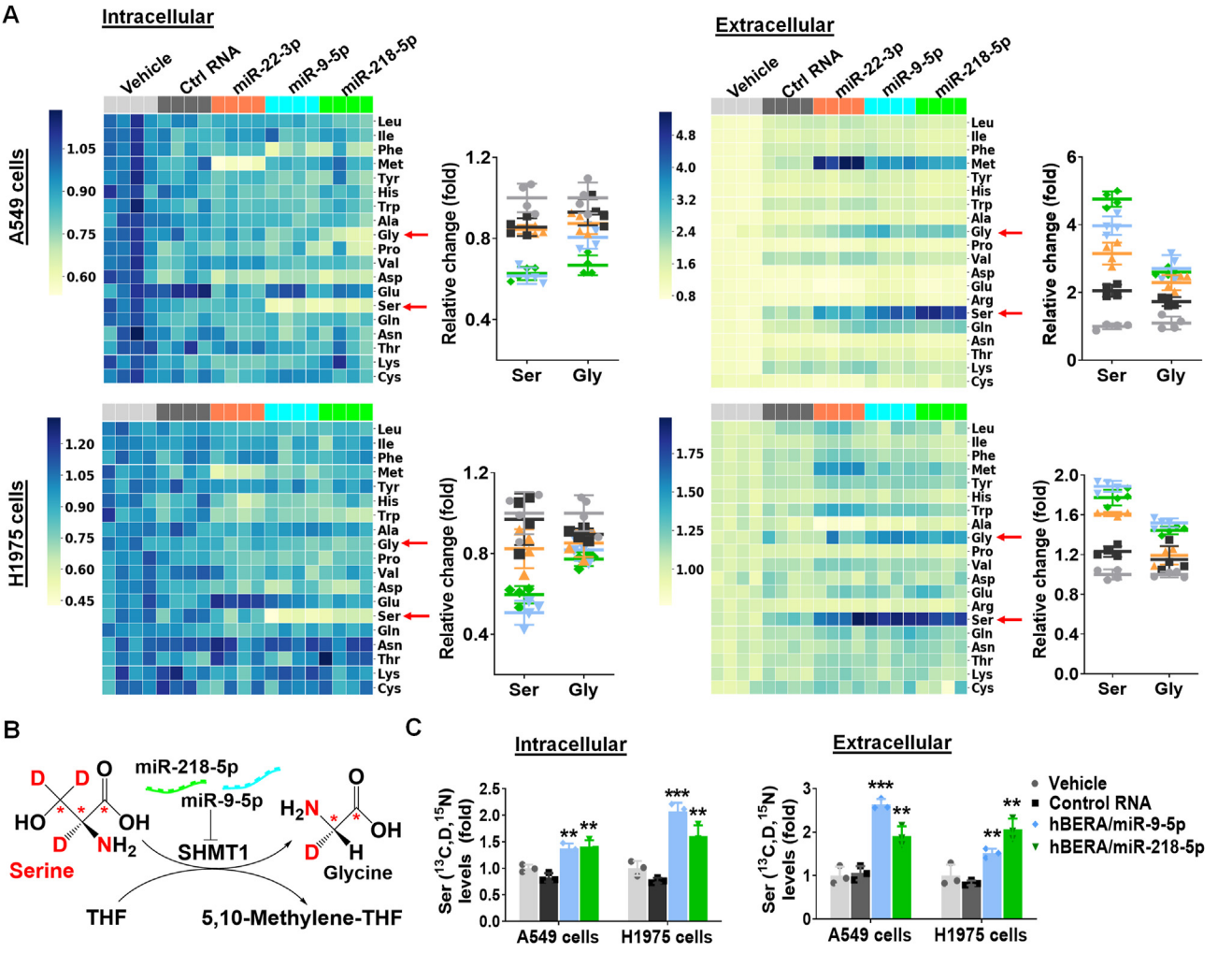


**Figure 4** MiR-22-3p, miR-9-5p, and miR-218-5p modulate amino acid metabolome intertwined with folate metabolism in human NSCLC cells. (A) Intracellular and extracellular amino acid levels were determined by LC−MS/MS analyses at 72 h after cells were treated with 15 nmol/L of biologic miRNAs, control RNA or vehicle. Values are mean ± SD ($n$ = 4/group). Among them, miR-9-5p and miR-218-5p showed greater impact on serine consumption while miR-22 influenced methionine homeostasis. (B) Schematic representation of serine depletion that is linked to SHMT1-mediated folate metabolism regulated by miR-9-5p and miR-218-5p. (C) Consumption of serine ($^{13}$C, D, $^{15}$N) were reduced in NSCLC cells following the treatment with 15 nmol/L of miRNAs. Media were supplemented with 10% of isotope-labeled serine ($^{13}$C, D, $^{15}$N). Serine concentrations were quantitated by selective LC−MS/MS method. Values are mean ± SD ($n$ = 4/group). $^{**}P < 0.01$ and $^{***}P < 0.001$, compared with control RNA (one- or two-way ANOVA with Bonferroni *post hoc* tests).

serine biosynthesis was inhibited, the mRNA levels of key serine biosynthesis enzymes were determined by qPCR analyses with gene selective primers (Supporting Information Table S5). The levels of *PHGDH* (D-3-phosphoglycerate dehydrogenase), *PSAT-1* (phosphoserine aminotransferase 1), and *PSPH* (phosphoserine phosphatase) in both A549 and H1975 cells were markedly downregulated by recombinant miR-9-5p and miR-218-5p, whereas none was altered by miR-22-3p (Fig. 5E). The results suggest that miR-9-5p and miR-218-5p modulate intracellular serine levels *via* the downregulation of serine biosynthesis enzymes. By contrast, miR-22-3p reduces intracellular supply of glucose through the suppression of GLUT1 protein outcome and subsequently, inhibits intracellular serine levels.

In view of the notable effects of three miRNAs on glucose uptake and metabolism, a glycolytic rate assay based on the Seahorse Real-time Cell Metabolic Analysis System was then conducted to examine whether NSCLC cell glycolysis capacity would be altered. Live cell proton efflux situations were monitored, and the glycolytic proton efflux rates (PER) were calculated after deducting mitochondrial contributions. The data showed that, in both A549 and H1975 cells, the three miRNAs all significantly suppressed the compensatory glycolysis, compared with control RNA or vehicle treatments (Fig. 5F). Among them, miR-22-3p was the most effective to reduce the compensatory glycolysis capacity of NSCLC cells (by around 50%−60%), similar as the findings on antifolate effects (Fig. 3).

### *3.6. MiR-22-3p is more effective than miR-9-5p and -218-5p to inhibit NSCLC cell proliferation and colony formation, which is associated with relatively greater degrees of cell cycle arrests and reduction of mitochondrial respiration*

To further compare the efficacy of three leading miRNAs in the inhibition of human NSCLC cell viability, individual dose

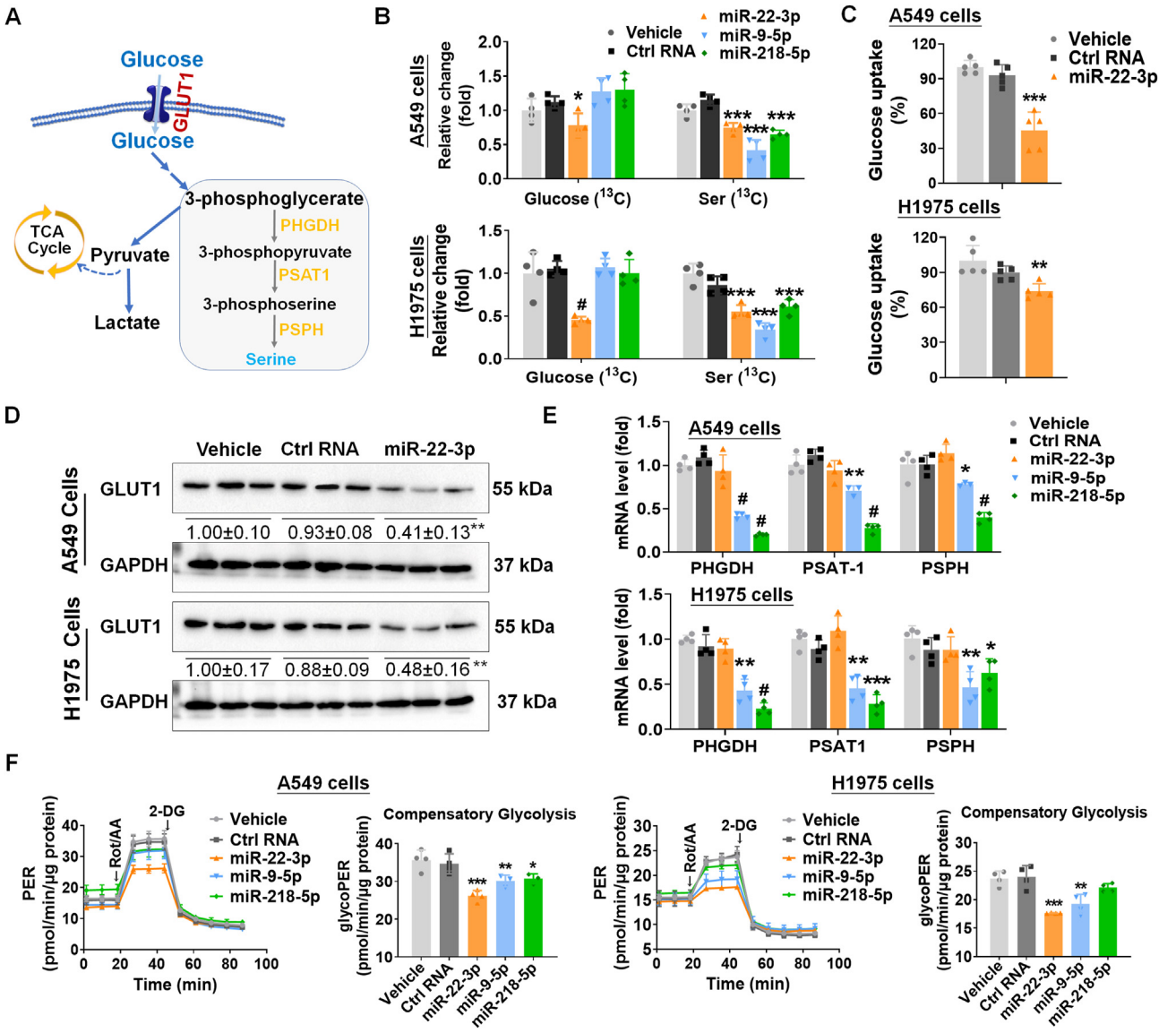


**Figure 5** MiR-22-3p reduces glucose uptake to alter glycolysis in human NSCLC cells, while miR-9-5p and miR-218-5p regulate serine biosynthesis. (A) Schematic representation of GLUT1-controlled glucose uptake, glycolysis pathway (to lactate), and serine biosynthesis from 3-phosphoglycerate. (B) Intracellular glucose ($^{13}$C) and serine ($^{13}$C) levels were determined by LC-MS/MS analyses following the treatment with 15 nmol/L of biologic miRNAs, control RNA or vehicle for 72 h, where glucose in the medium was replaced with uniformly $^{13}$C -labelled glucose. Values are mean ± SD ($n$ = 4/group). (C) Glucose uptake capacity was determined by the 2-NBDG-based glucose uptake assay in A549 and H1975 cells after treated with 15 nmol/L of miR-22-3p, control RNA or vehicle for 72 h. Values are mean ± SD ($n$ = 5/group). (D) GLUT1 protein levels were determined in cells by Western blot analyses after being treated with 15 nmol/L of biologic miR-22-3p, control RNA or vehicle for 72 h. GAPDH was used as a loading control, and values are mean ± SD ($n$ = 3/group). (E) The mRNA levels of serine synthetic enzymes, PHGDH, PSAT1, and PSPH, were determined in NSCLC cells by qPCR analyses, following 72 h exposure to 15 nmol/L of miRNAs, control RNA or vehicle. Values are mean ± SD ($n$ = 4/group). (F) Proton efflux rates (PER) of A549 and H1975 cells with different treatments were determined with Glycolysis Assay Kit on a Seahorse XFe24 live cell analyzer. Differences in compensatory glycolysis between miRNA and control groups were noted. Data were normalized to total protein levels, and values are mean ± SD ($n$ = 4/group). *$P$ < 0.05, **$P$ < 0.01, ***$P$ < 0.001, and $^{\#}P$ < 0.0001, compared with control RNA (one- or two-way ANOVA with Bonferroni *post hoc* tests).

response relationships were determined by using a CellTiter-Glo Luminescent cell viability assay. The results showed that miR-22-3p, -9-5p, and -218-5p all inhibited A549 and H1975 cell proliferation in a dose dependent manner (Supporting Information Fig. S5A). Among them, miR-22-3p exhibited the greatest potency that was readily indicated by its lowest $EC_{50}$ values (around 14 nmol/L) against both A549 and H1975 cells (Fig. S5B). Moreover, colony formation study on the two NSCLC cell lines confirmed that miR-22-3p was the most efficacious among the three biologic miRNAs to control the formation of colonies from single carcinoma cells (Fig. 6A). Flow cytometric analyses were then performed to determine how and to what degrees cell cycle profiles could be changed by the three miRNAs. Compared with control RNA or vehicle treatments, miR-22-3p, -9-5p, and -218-5p

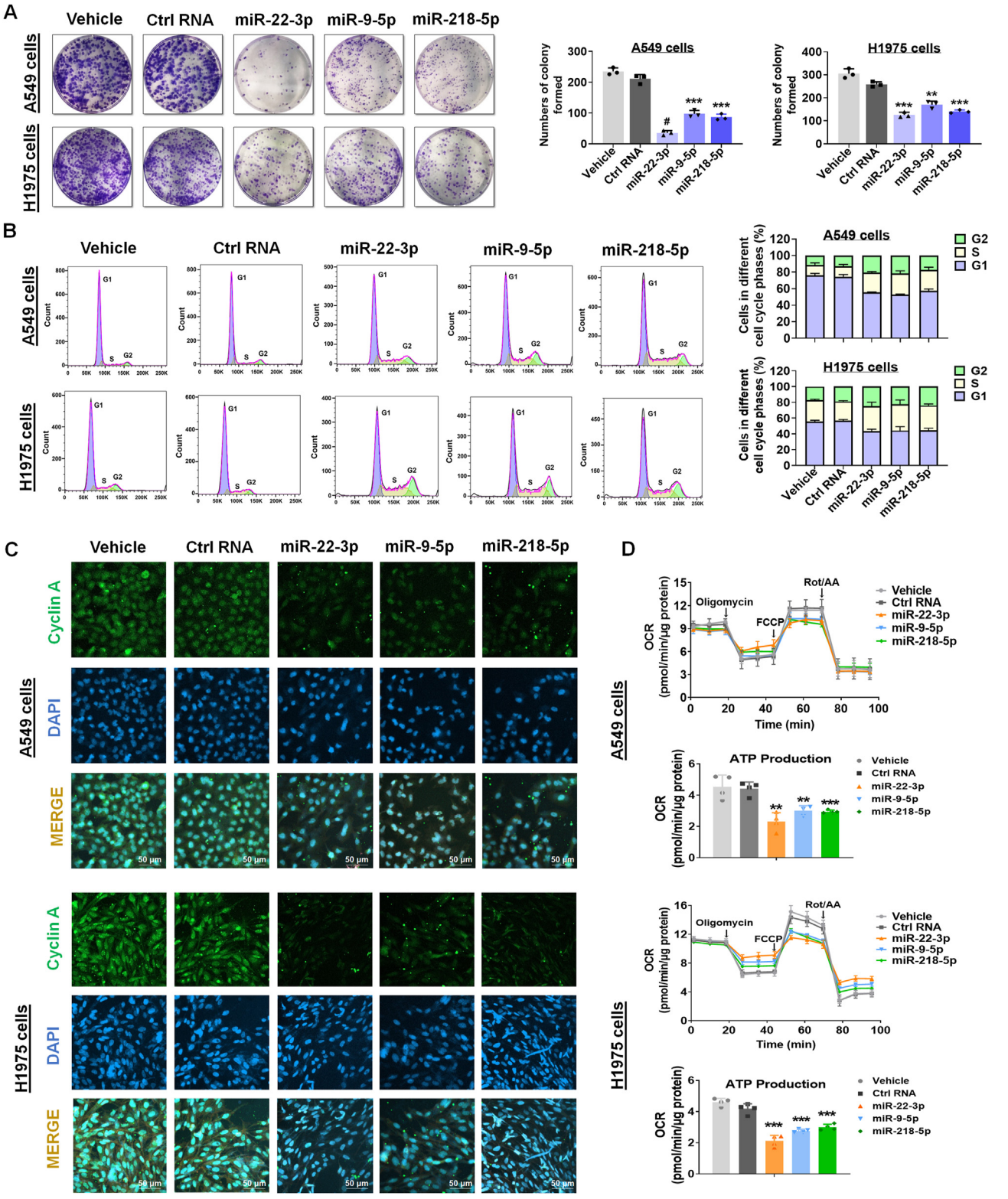


**Figure 6** Inhibition of NSCLC cell colony formation by miR-22-3p, miR-9-5p, and miR-218-5p is associated with the induction of cell cycle arrest and suppression of mitochondrial respiration. (A) Colony formation capacities of A549 and H1975 cells following the treatment with 15 nmol/L of hBERA/miRNAs, control RNA or vehicle. After cultured for additional 14 days, cells were stained with crystal violet for visualization. Values are mean ± SD ($n$ = 3/group). (B) Cell cycle stages were determined by flow cytometry analyses after cells were treated with 15 nmol/L of miRNAs, control RNA or vehicle, and stained with PI/RNase A solution. Values are mean ± SD ($n$ = 3/group). (C) Confocal images of cell cycle-related protein and cell proliferating marker Cyclin A fluorescence in A549 and H1975 cells after treated with 15 nmol/L of biologic miRNAs, control RNA or vehicle. (D) Real-time oxygen consumption rates (OCR) of NSCLC cells were determined with Mito Stress

all caused a dramatically accumulation of A549 and H1975 cells in the S and G2 phases, accompanied with a reduction of corresponding cells in the G1 phases (Fig. 6B). Additional immunofluorescence studies on Cyclin A2, one of the cell cycle regulators mainly expressed in the nucleus during the late S and G2 phases and being a useful marker for proliferating cells[59], revealed that the nuclear Cyclin A2 contents in both A549 and H1975 cells were obviously reduced after treated with individual miRNAs, as compared with control RNA or vehicle (Fig. 6C), indicating the suppression of cell proliferation by the miRNAs. Among them, miR-22-3p-treated cells exhibited the lowest extents of Cyclin A2 staining. These results indicate that miR-22-3p is the most potent among the three leading miRNAs in the inhibition of NSCLC cell proliferation and colony formation involving in the induction of G2 and S phase arrests.

Moreover, we examined the roles of these miRNAs in the modulation of NSCLC cell mitochondrial functions and influence on oxidative stress since mitochondrion is the major source of ROS, and mitochondrial respiratory dysfunction may lead to ROS accumulation and ROS-induced oxidative stress and apoptotic cell death[60,61]. Firstly, the real-time OCR of A549 and H1975 cells subjected to various treatments were determined by using a Seahorse analyzer and Cell Mito Stress Test Assay. The data showed that, compared to control RNA and vehicle treatments, ATP production in each cell line was markedly reduced by individual miRNAs, and to the greatest degree (>50%) by miR-22-3p (Fig. 6D). Meanwhile, recombinant miR-22-3p led to a more dramatical decrease of spare and maximal respiration capacity than miR-9-5p and -218-5p in both A549 and H1975 cells (Supporting Information Fig. S6A). Secondly, intracellular ROS levels were found to be significantly increased by the three miRNAs in NSCLC cells, and to the greatest levels by miR-22-3p (Fig. S6B). Rather, there was no statistical difference in the NADP/NADPH ratios between NCSLC cells treated with any of the three miRNAs and control RNA or vehicle (Fig. S6C). Collectively, these results demonstrate the roles of miR-22-3p, -9-5p, and -218-5p in the control of NSCLC cell mitochondrial respiration and ROS levels, among which miR-22-3p exhibits the highest activity.

### *3.7. Recombinant miR-22-3p therapy is effective and safe to control tumor growth in two NSCLC patient-derived xenograft (PDX) -mouse models*

Because miR-22-3p consistently displayed the greatest potency among the three lead miRNAs in the inhibition of NSCLC cell metabolism, respiration, proliferation, and colony formation, the effectiveness of recombinant miR-22-3p to control tumor progression was critically determined in two NSCLC PDX lines (LG-1202 and LG-0552F) *in vivo*. Compared to the control RNA treatment, biologic miR-22-3p therapy sharply suppressed the growth of both lines of PDX tumors (>50%) (Fig. 7A) which was further validated by visual inspection of the PDX tumor tissues excised from animals (Fig. 7B). Likewise, the tumor to body weight ratio in the miR-22-3p therapy group was found much lower than control RNA treatment (Fig. 7C), confirming the antitumor efficacy of miR-22-3p in the two PDX mouse models. Furthermore, much larger areas of necrosis were readily identified through histopathological examination of PDX tumor tissue sections from the miR-22-3p therapy groups, as compared to corresponding control RNA treatments (Fig. 7D), which was attributable to the inhibition of tumoral cell proliferation by miR-22-3p, as revealed by immunohistochemistry study on the Ki67 biomarker (Fig. 7E). In addition, Western blot analyses revealed that the protein levels of both MTHFR and MTHFD2, two direct targets of miR-22-3p involved in folate metabolism (Fig. 2), were significantly lower in the PDX tumor samples excised from mice treated with miR-22-3p than control RNA (Fig. 7F), supporting the on-target effects of therapeutic miR-22-3p *in vivo*. These results demonstrate the effectiveness of bioengineered miR-22-3p to inhibit tumor growth in NSCLC PDX mouse models.

Except one mouse within the LG0552F PDX line treated with control RNA found dead on Day 18, none of the animals showed any abnormal behaviors during the therapy studies, and the mouse body weights did not differ between miR-22-3p therapy and control RNA treatment groups, indicating that therapeutic miR-22-3p was well tolerated in the animals. Blood biochemistry profiles were further determined to evaluate the safety of biologic miR-22-3p therapeutics. Individual blood biomarkers related to liver and kidney functions, including alanine aminotransferase (ALT), aspartate aminotransferase (AST), albumin, total bilirubin, blood urea nitrogen (BUN), creatinine, and alkaline phosphatase (ALP), were all within the normal ranges. Moreover, there was no significant difference in any biomarker level between therapy and control groups in both PDX lines (Fig. 7G), indicating that miR-22-3p therapy did not induce any hepatic or renal toxicity.

## 4. Discussion

With an increased understanding of biological functions of miRNAs dysregulated in carcinoma cells, there are growing interests in developing novel miRNA-based therapies. Compared to the antagonism of tumor promotive miRNAs (*e.g.*, miR-21-5p and -205-5p) overexpressed in tumor with complementary oligonucleotides, reintroduction of tumor suppressive miRNAs (*e.g.*, miR-124-3p and let-7-5p) lost or downregulated in cancerous cells is more attractive because the reintroduced miRNAs could be more tolerable as normal human body ingredients[40,41]. Nevertheless, miRNA research and drug development are dominated by using miRNA mimics chemically synthesized *in vitro* and comprised of extensive and various forms of artificial modifications, which may not recapitulate the structures and physicochemical and biological properties of natural RNAs produced and folded in living cells[45]. Inspired by the success of recombinant protein research and therapy, we have made large efforts to develop novel approaches to achieve *in vivo* production of recombinant or bioengineered miRNA agents, which are a novel class of true biologic RNA molecules for research and development[42,43,46–49]. In the present study, we first identified six most effective miRNAs from a focused group of unique recombinant miRNA molecules in the inhibition of NSCLC cell viability *via* experimental screening, which were revealed to share a battery of pathways through bioinformatic analyses. This network indicates the enrichment of potential miRNA targets, in which many

Test kit on a Seahorse XFe24 Analyzer after treated with 15 nmol/L of miRNAs, control RNA or vehicle. Differences in ATP production were depicted. The data were normalized to respective total protein levels, and values are mean ± SD ($n$ = 4/group). $^{**}P < 0.01$, $^{***}P < 0.001$, $^{\#}P < 0.0001$, compared with control RNA (one-way ANOVA with Bonferroni *post hoc* tests).

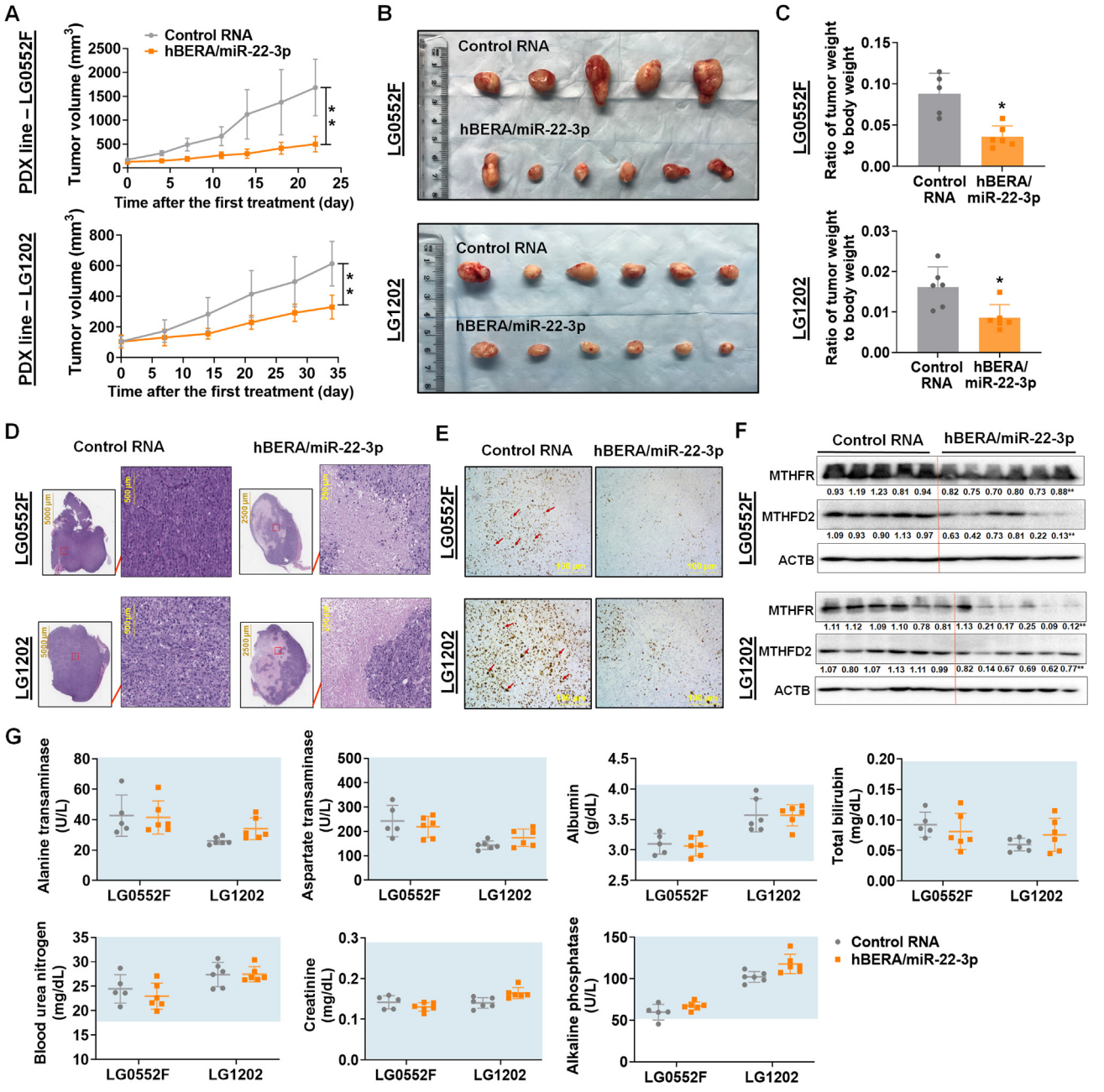


**Figure 7** Recombinant miR-22-3p therapy in two NSCLC patient-derived xenograft (PDX) mouse models *in vivo*. (A) Tumor growth curves after mice were treated with LPP-formulated hBERA/miR-22-3p or control RNA. Values are mean ± SD ($n$ = 6/group, except that one mouse within the LG0552F PDX control treatment group found dead on Day 18). (B) Visual comparison of PDX tumors dissected from individual mice. (C) The ratios of tumor over mouse body weights between miR-22-3p therapy and control RNA group were compared. Values are mean ± SD ($n$ = 5 or 6 per group). (D) Images of H&E-stained PDX tumor sections subjected to different treatments. (E) Immunohistochemistry analyses of Ki67 indicating PDX tumoral cell proliferation in different treatment groups. (F) MTHFR and MTHFD2 protein levels within individual tumors were determined by Western blot analyses. ACTB was used as a loading control, and protein levels were normalized to control RNA group for comparison. Data are mean ± SD ($n$ = 5 or 6 per group). (G) Blood chemistry profiles, including alanine transaminase (ALT), aspartate transaminase (AST), albumin, total bilirubin, blood urea nitrogen (BUN), creatinine, and alkaline phosphatase (ALP), were not statistically significant ($P > 0.05$) between miR-22-3p- and control RNA-treated tumor-bearing mice. The guideline ranges of individual markers (derived from BALB/c mice by the Comparative Pathology Laboratory at UC Davis) are marked as references. *$P < 0.05$ and **$P < 0.01$, compared with Control RNA (one- or two-way ANOVA with Bonferroni *post hoc* tests).

are assembled into a dominant cluster of cellular energy metabolism pathways, including one carbon pool by folate and the biosynthesis or metabolism of amino acids that are experimentally validated in this study.

Folate one-carbon metabolism, catalyzed specifically by SHMT, incorporates the one-carbon methylene group from serine into folate cycle that are connected to series of bio-transformations towards the production of nucleic acids essential

for cell survival and proliferation[8]. Meanwhile, some other critical cellular processes such as amino acid synthesis and redox reactions are closely regulated by folate one-carbon metabolism[8,9]. Inhibition of folate metabolism is also a well-established mechanism of action for several existing anticancer medications (*e.g.*, methotrexate and pemetrexed), and a few miRNAs (*e.g.*, miR-22-3p and miR-940-5p) have been showed to regulate folate metabolism in carcinoma cells (*e.g.*, breast and glioma, respectively)[24,62]. After folate one-carbon metabolism was identified as a potential common pathway for three lead antiproliferative miRNAs, miR-22-3p, -9-5p, and -218-5p, current study systemically validated multiple folate metabolic enzyme-encoding genes as direct targets for individual miRNAs and defined the impact on protein outcomes in NSCLC cells, including SHMT1 and MTHFD2 and MTHFD1L for miR-9-5p, MTHFR and MTHFD2 for miR-22-3p, and SHMT1 for miR-218-5p, although some were studied previously in other diseases or different types of cancer[63–66]. As a result, bioengineered miR-22-3p, -9-5p, and -218-5p were all effective to suppress folate metabolism, as manifested by sharp accumulation of folic acid and DHF within both A549 and H1975 cells. The reduction of folic acid and DHF consumption was also consistent with the finding on suppression of the production of respective folate metabolite in cells, 5-methyl-THF, 5,10-methenyl-THF, and 5-formyl-THF, all to the greatest degrees by miR-22-3p. Most importantly, isotope tracing study directly demonstrated the repression of transferring the methylene bridge from serine to folate metabolites, 5-methyl-THF (M+3) and 5,10-methenyl-THF (M+2), by miR-22-3p, -9-5p, and -218-5p in NSCLC cells, supporting the interference with folate one-carbon metabolism as a common mechanism for the three lead antiproliferative miRNAs, amid miR-22-3p exhibiting the highest antifolate activity.

Folate cycle is intertwined with amino acid metabolism[8,57], which consists of some proved or promising therapeutic targets in cancer[58]. The present study disclosed that the three lead miRNAs, in addition to the disruption of folate metabolism in NSCLC cells, interfered with amino acid metabolome that was manifested by remarkable increases in extracellular serine and methionine levels. The reduction of serine consumption by miR-9-5p and miR-218-5p was further verified by feeding study with isotope-labeled serine, consistent with the suppression of SHMT1 expression and simultaneously blocking the conversion of THF to 5,10-methylene-THF. By contrast, miR-22-3p seemed to mainly repress methionine consumption by NSCLC cells, which, along with its induction of cell cycle arrest identified in this study, is consistent with previous finding on tumor-specific G2/S arrest under methionine restriction[67]. Anyhow, antifolate itself may cause the inhibition of nucleoside (*e.g.*, purine and thymidine) and thus DNA synthesis, leading to cell cycle arrest in the S phase and thus cell proliferation as revealed by various methods in this study, despite that contribution from other possible mechanisms cannot be excluded. In addition to being a building block for protein synthesis as well as a precursor for cysteine and polyamine synthesis, methionine is essential to produce *S*-adenosylmethionine that serves as a sole methyl donor for the methylation of biological molecules. While the precise mechanism by which extracellular methionine levels were increased following miR-22-3p treatment awaits further investigation, the reduction of intracellular methionine by miR-22-3p is likely due to the downregulation of MTHFR, the rate-limiting enzyme in the methyl cycle while concurrently converting 5,10-methylenetetrahydrofolate to 5-methyltetrahydrofolate[68]. In any cases, our new findings on the reduction of serine and methionine consumption by tumor suppressive miRNAs is in line with the concept of amino acid restriction or depletion therapy for the treatment of cancer diseases[58].

However, endogenous serine levels were surprisingly lower within cells treated with miR-9-5p and -218-5p, which aroused our further study on serine biosynthesis from glucose by feeding $^{13}$C-labeled glucose. Indeed, miR-9-5p and -218-5p decreased the production of corresponding $^{13}$C-labeled serine from $^{13}$C-labeled glucose, associated with the reduction of mRNA levels of serine biosynthetic enzymes (*PHGDH*, *PSAT-1*, and *PSPH* ). As these serine synthetase-encoding genes are not computationally predicted targets of miR-9-5p and -218-5p, they might be indirectly altered by the two miRNAs through affecting their upstream transcription factors, such as the NRF2 and ATF4 regulatory factors having been showed to control transcriptional gene expression of serine enzymes PHGDH, PSAT1 and SHMT2[69], which rather warrants more extensive investigation. By contrast, miR-22-3p was revealed to reduce serine biosynthesis through the suppression of glucose uptake. This is attributable to the downregulation of GLUT1 by miR-22-3p in NSCLC cells, consistent with previous finding on miR-22-controlled regulation of GLUT1 in breast cancer cells[23]. In concordance with previous report on the inhibition of glycolysis by folate restriction[70], the reduction of glycolysis by the three miRNAs agrees with their antifolate functions in NSCLC cells reported in this study. In addition, similar as antifolate effects, miR-22-3p showed the greatest antiglycolytic activity which can be interpreted by its direct action on GLUT1-mediated glucose uptake. Therefore, miR-22-3p represents a more general modulator of cancer metabolism.

Likewise, miR-22-3p was revealed to be the most effective among the three lead miRNAs in the control of NSCLC cell growth phenotypes, such as proliferation and colony formation. Indeed, folate metabolism offers essential components such as purine and thymidine for nucleic acid biosynthesis that is closely related to DNA replication and cell cycle[8]. Therefore, antifolate agents commonly induce cell cycle arrest to exhibit antiproliferative activities. Our findings on the induction of arrest of DNA synthesis phase and decrease of proliferating-cell marker Cyclin A2 levels by three antifolate miRNAs indicate the disruption of nucleotide synthesis materials and explains their anti-proliferation and anti-colony formation activities. Furthermore, the folate one-carbon metabolism includes both cytoplasmic and mitochondrial components linking serine to formate shuttling between the two organelles[9,57]. Therefore, the determination of changes in mitochondrial respiration in current study provides insights into understanding the impact of the three lead miRNAs on NSCLC energetics beyond glycolysis, which also supports the complexity of cancer metabolism[57] and need for comprehensive evaluations of the actions of an agent of interest, such as miR-22-3p, -9-5p, and -218-5p herein. The inhibition of mitochondrial function by the three lead miRNAs was also accompanied by an enhanced ROS accumulation in NSCLC cells, to a greater degree by miR-22-3p than miR-9-5p and -218-5p, consistent with their antifolate, anti-glycolysis, anti-proliferation, and anti-colony formation activities.

Compared to cell line-derived xenograft mouse models, the PDX models that could better simulate the properties of original cancer patients and reflect the efficacy of treatments, have been increasingly used for cancer research and development of new therapies. Accordingly, two NSCLC PDX models were established and utilized in this study to define the therapeutic efficacy of miR-22-3p. To improve the pharmacokinetics of therapeutic RNA, a newly developed liposome-polyethylenimine nanocomplex (lipopolyplex or

LPP) was employed to formulate recombinant miR-22-3p nanomedicine. The LPP integrates the benefits of lipid and polyethylenimine (PEI) systems, and significantly reduces PEI component and toxicities[55]. Our recent studies have also demonstrated that LPP provided efficient delivery of bioengineered RNAs to lung, liver, and tumor tissues in mouse models[48,49]. In this study, miR-22-3p LPP nanomedicine was shown to significantly inhibit NSCLC tumor progression in both PDX lines, albeit with a relatively small sample size. The antitumor efficacy of miR-22-3p was associated with a sharp reduction of tumor cell proliferation, as well as lower levels of tumoral MTHFR and MTHFD2 proteins. The latter not only indicates the on-target effects of therapeutic miR-22-3p but also support the antifolate mechanism of action behind its antitumor efficacy. It is noteworthy that the two PDX lines unsurprisingly showed variable aggressiveness and sensitivities. The LG-0552F PDX tumors are highly malignant and grow faster, which limited a shorter period of therapy study with six doses before reaching the humane endpoint. In addition, recombinant miR-22-3p LPP therapy was well tolerated in the subjects without causing any hepatic or renal toxicity. Nevertheless, more extensive studies are necessary to critically determine the safety and efficacy of therapeutic miRNAs in other animal models such as nonhuman primates, as well as possible involvement of other mechanisms besides antifolate actions.

## 5. Conclusions

Through experimental screening of unparalleled recombinant miRNA agents and bioinformatic analyses, folate one-carbon metabolism was identified as a common action for three lead antiproliferative miRNAs, miR-22-3p, -9-5p, and -218-5p. The effects of individual miRNAs in the modulation of respective folate metabolic enzymes (SHMT1, MTHFR, MTHFD2, MTHFD1L) and control of folate metabolism in NSCLC cells were explicitly determined. Isotope tracing studies further confirmed the disruption of one-carbon transfer from serine to folate cycle, as well as glucose uptake and biotransformation to serine by individual miRNAs. Besides showing the greatest antifolate activity among the three lead miRNAs, miR-22-3p exhibited the highest activities in the inhibition of NSCLC cell glycolysis, respiration, proliferation, and colony formation. In addition, recombinant miR-22-3p nanomedicine was effective and safe to control tumor growth in two NSCLC PDX mouse models, associated with on-target molecular and cellular mechanism of action. These results demonstrate antifolate actions for multiple oncolytic miRNAs, suggest folate metabolism a crucial pathway in NSCLC cells, and provide insights into developing new therapies for NSCLC.

## Acknowledgments

This study was supported in part by the National Cancer Institute [R01CA225958 and R01253230] and National Institute of General Medical Sciences [R35GM140835], National Institutes of Health (USA). Huichang Bi was supported by grants from the Chinese National Key Research and Development Program (2017YFE0109900, China). Yixin Chen was supported by a scholarship from the Chinese Scholarship Council (No. 201806380133, China). The authors appreciate the access to the Molecular Pharmacology, Flow Cytometry, and Mouse Biology Shared Resources funded by the UC Davis Comprehensive Cancer Center Support Grant awarded by the National Cancer Institute (P30CA093373), National Institutes of Health.

## Author contributions

Ai-Ming Yu, Yixin Chen, and all other authors participated in research design. Yixin Chen, Mei-Juan Tu, Fangwei Han, Zhenzhen Liu, and Neelu Batra conducted the experiments and data analyses. Yixin Chen, Ai-Ming Yu, and all other authors contributed to data interpretation and writing of the manuscript. All authors have read and agreed to the final version of the manuscript. The authors declare no conflicts of interest.

## Conflicts of interest

Ai-Ming Yu and Mei-Juan Tu are inventors of several granted and pending patents related to recombinant RNA technologies and uses that are owned by the UC Davis Research Foundation. Ai-Ming Yu is a founder of AimRNA, Inc. that intends to license the intellectual property to develop RNA technologies and therapeutics. The authors are responsible for the content and writing of this article.

## Appendix A. Supporting information

Supporting data to this article can be found online at https://doi.org/10.1016/j.apsb.2023.07.011.

## References

1. Siegel RL, Miller KD, Fuchs HE, Jemal A. Cancer statistics, 2022. *CA Cancer J Clin* 2022;**72**:7−33.
2. Sung H, Ferlay J, Siegel RL, Laversanne M, Soerjomataram I, Jemal A, et al. Global cancer statistics 2020: GLOBOCAN estimates of incidence and mortality worldwide for 36 cancers in 185 countries. *CA Cancer J Clin* 2021;**71**:209−49.
3. Duma N, Santana-Davila R, Molina JR. Non-small cell lung cancer: epidemiology, screening, diagnosis, and treatment. *Mayo Clin Proc* 2019;**94**:1623−40.
4. Herbst RS, Morgensztern D, Boshoff C. The biology and management of non-small cell lung cancer. *Nature* 2018;**553**:446−54.
5. Yu Z, Zhou X, Wang X. Metabolic reprogramming in hematologic malignancies: advances and clinical perspectives. *Cancer Res* 2022;**82**:2955−63.
6. Vander Heiden MG, Cantley LC, Thompson CB. Understanding the Warburg effect: the metabolic requirements of cell proliferation. *Science* 2009;**324**:1029−33.
7. Martinez-Outschoorn UE, Peiris-Pages M, Pestell RG, Sotgia F, Lisanti MP. Cancer metabolism: a therapeutic perspective. *Nat Rev Clin Oncol* 2017;**14**:11−31.
8. Ducker GS, Rabinowitz JD. One-carbon metabolism in health and disease. *Cell Metab* 2017;**25**:27−42.
9. Newman AC, Maddocks ODK. One-carbon metabolism in cancer. *Br J Cancer* 2017;**116**:1499−504.
10. Rajagopalan PT, Zhang Z, McCourt L, Dwyer M, Benkovic SJ, Hammes GG. Interaction of dihydrofolate reductase with methotrexate: ensemble and single-molecule kinetics. *Proc Natl Acad Sci U S A* 2002;**99**:13481−6.
11. Longley DB, Harkin DP, Johnston PG. 5-Fluorouracil: mechanisms of action and clinical strategies. *Nat Rev Cancer* 2003;**3**:330−8.
12. Manegold C. Pemetrexed: its promise in treating non-small-cell lung cancer. *Oncology* 2004;**18**:43−8.

13. Robinson AD, Eich ML, Varambally S. Dysregulation of *de novo* nucleotide biosynthetic pathway enzymes in cancer and targeting opportunities. *Cancer Lett* 2020;**470**:134−40.
14. Zhong S, Golpon H, Zardo P, Borlak J. miRNAs in lung cancer. A systematic review identifies predictive and prognostic miRNA candidates for precision medicine in lung cancer. *Transl Res* 2021;**230**: 164−96.
15. Liu J, Ren L, Li S, Li W, Zheng X, Yang Y, et al. The biology, function, and applications of exosomes in cancer. *Acta Pharm Sin B* 2021;**11**:2783−97.
16. Petrek H, Yu AM. MicroRNAs in non-small cell lung cancer: gene regulation, impact on cancer cellular processes, and therapeutic potential. *Pharmacol Res Perspect* 2019;**7**:e00528.
17. Ambros V. The functions of animal microRNAs. *Nature* 2004;**431**: 350−5.
18. Li X, Carthew RW. A microRNA mediates EGF receptor signaling and promotes photoreceptor differentiation in the drosophila eye. *Cell* 2005;**123**:1267−77.
19. Chen R, Qian Z, Xu X, Zhang C, Niu Y, Wang Z, et al. Exosomes-transmitted miR-7 reverses gefitinib resistance by targeting YAP in non-small-cell lung cancer. *Pharmacol Res* 2021;**165**:105442.
20. Azizi M, Othman I, Naidu R. The role of MicroRNAs in lung cancer metabolism. *Cancers* 2021;**13**:1716.
21. Lu J, Zhan Y, Feng J, Luo J, Fan S. MicroRNAs associated with therapy of non-small cell lung cancer. *Int J Biol Sci* 2018;**14**:390−7.
22. Yi C, Yu AM. MicroRNAs in the regulation of solute carrier proteins behind xenobiotic and nutrient transport in cells. *Front Mol Biosci* 2022;**9**:893846.
23. Chen B, Tang H, Liu X, Liu P, Yang L, Xie X, et al. miR-22 as a prognostic factor targets glucose transporter protein type 1 in breast cancer. *Cancer Lett* 2015;**356**:410−7.
24. Koufaris C, Valbuena GN, Pomyen Y, Tredwell GD, Nevedomskaya E, Lau CH, et al. Systematic integration of molecular profiles identifies miR-22 as a regulator of lipid and folate metabolism in breast cancer cells. *Oncogene* 2016;**35**:2766−76.
25. Xiong S, Zheng Y, Jiang P, Liu R, Liu X, Qian J, et al. PA28gamma emerges as a novel functional target of tumour suppressor microRNA-7 in non-small-cell lung cancer. *Br J Cancer* 2014;**110**:353−62.
26. Deng B, Sun Z, Jason W, Yang P. Increased BCAR1 predicts poor outcomes of non-small cell lung cancer in multiple-center patients. *Ann Surg Oncol* 2013;**20**(Suppl 3):S701−8.
27. Ma DJ, Zhou XY, Qin YZ, Tian ZH, Liu HS, Li SQ. MiR-22-3p expression is down-regulated in lung adenocarcinoma. *Acta Biochim Pol* 2021;**68**:667−72.
28. Yang X, Su W, Li Y, Zhou Z, Zhou Y, Shan H, et al. MiR-22-3p suppresses cell growth *via* MET/STAT3 signaling in lung cancer. *Am J Transl Res* 2021;**13**:1221−32.
29. Li X, Yu Z, Li Y, Liu S, Gao C, Hou X, et al. The tumor suppressor miR-124 inhibits cell proliferation by targeting STAT3 and functions as a prognostic marker for postoperative NSCLC patients. *Int J Oncol* 2015;**46**:798−808.
30. Zu L, Xue Y, Wang J, Fu Y, Wang X, Xiao G, et al. The feedback loop between miR-124 and TGF-beta pathway plays a significant role in non-small cell lung cancer metastasis. *Carcinogenesis* 2016;**37**:333−43.
31. Johnson SM, Grosshans H, Shingara J, Byrom M, Jarvis R, Cheng A, et al. RAS is regulated by the let-7 microRNA family. *Cell* 2005;**120**: 635−47.
32. Zhao B, Han H, Chen J, Zhang Z, Li S, Fang F, et al. MicroRNA let-7c inhibits migration and invasion of human non-small cell lung cancer by targeting ITGB3 and MAP4K3. *Cancer Lett* 2014;**342**:43−51.
33. Zhu K, Ding H, Wang W, Liao Z, Fu Z, Hong Y, et al. Tumor-suppressive miR-218-5p inhibits cancer cell proliferation and migration *via* EGFR in non-small cell lung cancer. *Oncotarget* 2016;**7**: 28075−85.
34. Shi ZM, Wang L, Shen H, Jiang CF, Ge X, Li DM, et al. Down-regulation of miR-218 contributes to epithelial−mesenchymal transition and tumor metastasis in lung cancer by targeting Slug/ZEB2 signaling. *Oncogene* 2017;**36**:2577−88.
35. Chen G, Wang Q, Wang K. MicroRNA-218-5p affects lung adenocarcinoma progression through targeting endoplasmic reticulum oxidoreductase 1 alpha. *Bioengineered* 2022;**13**:10061−70.
36. Muraoka T, Soh J, Toyooka S, Maki Y, Shien K, Furukawa M, et al. Impact of aberrant methylation of microRNA-9 family members on non-small cell lung cancers. *Mol Clin Oncol* 2013;**1**:185−9.
37. Nourmohammadi B, Tafsiri E, Rahimi A, Nourmohammadi Z, Daneshvar Kakhaki A, Cho W, et al. Expression of miR-9 and miR-200c, ZEB1, ZEB2 and E-cadherin in non-small cell lung cancers in Iran. *Asian Pac J Cancer Prev APJCP* 2019;**20**:1633−9.
38. Li G, Wu F, Yang H, Deng X, Yuan Y. MiR-9-5p promotes cell growth and metastasis in non-small cell lung cancer through the repression of TGFBR2. *Biomed Pharmacother* 2017;**96**:1170−8.
39. Yu AM, Tu MJ. Deliver the promise: RNAs as a new class of molecular entities for therapy and vaccination. *Pharmacol Ther* 2022; **230**:107967.
40. Yu AM, Choi YH, Tu MJ. RNA drugs and RNA targets for small molecules: principles, progress, and challenges. *Pharmacol Rev* 2020; **72**:862−98.
41. Bader AG, Brown D, Winkler M. The promise of microRNA replacement therapy. *Cancer Res* 2010;**70**:7027−30.
42. Ho PY, Duan Z, Batra N, Jilek JL, Tu MJ, Qiu JX, et al. Bioengineered noncoding RNAs selectively change cellular miRNome profiles for cancer therapy. *J Pharmacol Exp Therapeut* 2018;**365**: 494−506.
43. Wang WP, Ho PY, Chen QX, Addepalli B, Limbach PA, Li MM, et al. Bioengineering novel chimeric microRNA-34a for prodrug cancer therapy: high-yield expression and purification, and structural and functional characterization. *J Pharmacol Exp Therapeut* 2015;**354**: 131−41.
44. Li MM, Addepalli B, Tu MJ, Chen QX, Wang WP, Limbach PA, et al. Chimeric microRNA-1291 biosynthesized efficiently in *Escherichia coli* is effective to reduce target gene expression in human carcinoma cells and improve chemosensitivity. *Drug Metab Dispos* 2015;**43**: 1129−36.
45. Yu AM, Batra N, Tu MJ, Sweeney C. Novel approaches for efficient *in vivo* fermentation production of noncoding RNAs. *Appl Microbiol Biotechnol* 2020;**104**:1927−37.
46. Li PC, Tu MJ, Ho PY, Batra N, Tran MML, Qiu JX, et al. *In vivo* fermentation production of humanized noncoding RNAs carrying payload miRNAs for targeted anticancer therapy. *Theranostics* 2021; **11**:4858−71.
47. Deng L, Petrek H, Tu MJ, Batra N, Yu AX, Yu AM. Bioengineered miR-124-3p prodrug selectively alters the proteome of human carcinoma cells to control multiple cellular components and lung metastasis *in vivo*. *Acta Pharm Sin B* 2021;**11**:3950−65.
48. Petrek H, Yan Ho P, Batra N, Tu MJ, Zhang Q, Qiu JX, et al. Single bioengineered ncRNA molecule for dual-targeting toward the control of non-small cell lung cancer patient-derived xenograft tumor growth. *Biochem Pharmacol* 2021;**189**:114392.
49. Jilek JL, Zhang QY, Tu MJ, Ho PY, Duan Z, Qiu JX, et al. Bioengineered Let-7c inhibits orthotopic hepatocellular carcinoma and improves overall survival with minimal immunogenicity. *Mol Ther Nucleic Acids* 2019;**14**:498−508.
50. Umeh-Garcia M, Simion C, Ho PY, Batra N, Berg AL, Carraway KL, et al. A novel bioengineered miR-127 prodrug suppresses the growth and metastatic potential of triple-negative breast cancer cells. *Cancer Res* 2020;**80**:418−29.
51. Yi W, Tu MJ, Liu Z, Zhang C, Batra N, Yu AX, et al. Bioengineered miR-328-3p modulates GLUT1-mediated glucose uptake and metabolism to exert synergistic antiproliferative effects with chemotherapeutics. *Acta Pharm Sin B* 2020;**10**:1 59−70.
52. Nandania J, Kokkonen M, Euro L, Velagapudi V. Simultaneous measurement of folate cycle intermediates in different biological matrices using liquid chromatography-tandem mass spectrometry. *J Chromatogr B Anal Technol Biomed Life Sci* 2018;**1092**:168−78.
53. Liu Z, Tu MJ, Zhang C, Jilek JL, Zhang QY, Yu AM. A reliable LC−MS/MS method for the quantification of natural amino acids in

mouse plasma: method validation and application to a study on amino acid dynamics during hepatocellular carcinoma progression. *J Chromatogr B Anal Technol Biomed Life Sci* 2019;**1124**:72−81.
54. Tu MJ, Duan Z, Liu Z, Zhang C, Bold RJ, Gonzalez FJ, et al. MicroRNA-1291-5p sensitizes pancreatic carcinoma cells to arginine deprivation and chemotherapy through the regulation of arginolysis and glycolysis. *Mol Pharmacol* 2020;**98**:686−94.
55. Zhang QY, Ho PY, Tu MJ, Jilek JL, Chen QX, Zeng S, et al. Lipidation of polyethylenimine-based polyplex increases serum stability of bioengineered RNAi agents and offers more consistent tumoral gene knockdown *in vivo*. *Int J Pharm* 2018;**547**:537−44.
56. Chen L, Ducker GS, Lu W, Teng X, Rabinowitz JD. An LC−MS chemical derivatization method for the measurement of five different one-carbon states of cellular tetrahydrofolate. *Anal Bioanal Chem* 2017;**409**:5955−64.
57. Reina-Campos M, Diaz-Meco MT, Moscat J. The complexity of the serine glycine one-carbon pathway in cancer. *J Cell Biol* 2020;**219**:20190722.
58. Butler M, van der Meer LT, van Leeuwen FN. Amino acid depletion therapies: starving cancer cells to death. *Trends Endocrinol Metabol* 2021;**32**:367−81.
59. Poikonen P, Sjostrom J, Amini RM, Villman K, Ahlgren J, Blomqvist C. Cyclin A as a marker for prognosis and chemotherapy response in advanced breast cancer. *Br J Cancer* 2005;**93**:515−9.
60. Andreyev AY, Kushnareva YE, Starkov A. Mitochondrial metabolism of reactive oxygen species. *Biochemistry* 2005;**70**:200−14.
61. Sinha K, Das J, Pal PB, Sil PC. Oxidative stress: the mitochondria-dependent and mitochondria-independent pathways of apoptosis. *Arch Toxicol* 2013;**87**:1157−80.
62. Xu T, Zhang K, Shi J, Huang B, Wang X, Qian K, et al. MicroRNA-940 inhibits glioma progression by blocking mitochondrial folate metabolism through targeting of MTHFD2. *Am J Cancer Res* 2019;**9**:250−69.
63. Li C, Ni J, Liu YX, Wang H, Liang ZQ, Wang X. Response of miRNA-22-3p and miRNA-149-5p to folate deficiency and the differential regulation of MTHFR expression in normal and cancerous human hepatocytes. *PLoS One* 2017;**12**:e0168049.
64. Selcuklu SD, Donoghue MT, Rehmet K, de Souza Gomes M, Fort A, Kovvuru P, et al. MicroRNA-9 inhibition of cell proliferation and identification of novel miR-9 targets by transcriptome profiling in breast cancer cells. *J Biol Chem* 2012;**287**:29516−28.
65. Tong D, Zhang J, Wang X, Li Q, Liu L, Lu A, et al. MiR-22, regulated by MeCP2, suppresses gastric cancer cell proliferation by inducing a deficiency in endogenous *S*-adenosylmethionine. *Oncogenesis* 2020;**9**:99.
66. Yang Q, Li J, Hu Y, Tang X, Yu L, Dong L, et al. MiR-218-5p suppresses the killing effect of natural killer cell to lung adenocarcinoma by targeting SHMT1. *Yonsei Med J* 2019;**60**:500−8.
67. Hoffman RM, Yano S. Tumor-specific S/G2-phase cell cycle arrest of cancer cells by methionine restriction. *Methods Mol Biol* 2019;**1866**:49−60.
68. Su A, Ling F, Vaganay C, Sodaro G, Benaksas C, Dal Bello R, et al. The folate cycle enzyme MTHFR is a critical regulator of cell response to MYC-targeting therapies. *Cancer Discov* 2020;**10**:1894−911.
69. DeNicola GM, Chen PH, Mullarky E, Sudderth JA, Hu Z, Wu D, et al. NRF2 regulates serine biosynthesis in non-small cell lung cancer. *Nat Genet* 2015;**47**:1475−81.
70. Ashkavand Z, O'Flanagan C, Hennig M, Du X, Hursting SD, Krupenko SA. Metabolic reprogramming by folate restriction leads to a less aggressive cancer phenotype. *Mol Cancer Res* 2017;**15**:189−200.